

On: 14 April 2015, At: 00:20

Publisher: Taylor & Francis

Informa Ltd Registered in England and Wales Registered Number: 1072954 Registered office: Mortimer House, 37-41 Mortimer Street, London W1T 3JH, UK



Journal of Adhesion Science and Technology

Publication details, including instructions for authors and subscription information:

<http://www.tandfonline.com/loi/tast20>

Optimisation of interface roughness and coating thickness to maximise coating-substrate adhesion - a failure prediction and reliability assessment modelling

M.H. Nazir^a, Z.A. Khan^a & K. Stokes^b

^a Bournemouth University, Sustainable Design Research Centre (SDRC), Faculty of Science and Technology, Bournemouth, BH12 5BB, UK

^b Defence Science and Technology Laboratory (DSTL), Salisbury, UK

Published online: 13 Apr 2015.



[Click for updates](#)

To cite this article: M.H. Nazir, Z.A. Khan & K. Stokes (2015): Optimisation of interface roughness and coating thickness to maximise coating-substrate adhesion - a failure prediction and reliability assessment modelling, Journal of Adhesion Science and Technology, DOI: [10.1080/01694243.2015.1026870](https://doi.org/10.1080/01694243.2015.1026870)

To link to this article: <http://dx.doi.org/10.1080/01694243.2015.1026870>

PLEASE SCROLL DOWN FOR ARTICLE

Taylor & Francis makes every effort to ensure the accuracy of all the information (the "Content") contained in the publications on our platform. Taylor & Francis, our agents, and our licensors make no representations or warranties whatsoever as to the accuracy, completeness, or suitability for any purpose of the Content. Versions of published Taylor & Francis and Routledge Open articles and Taylor & Francis and Routledge Open Select articles posted to institutional or subject repositories or any other third-party website are without warranty from Taylor & Francis of any kind, either expressed or implied, including, but not limited to, warranties of merchantability, fitness for a particular purpose, or non-infringement. Any opinions and views expressed in this article are the opinions and views of the authors, and are not the views of or endorsed by Taylor & Francis. The accuracy of the Content should not be relied upon and should be independently verified with primary sources of information. Taylor & Francis shall not be liable for any losses, actions, claims, proceedings, demands, costs, expenses, damages,

and other liabilities whatsoever or howsoever caused arising directly or indirectly in connection with, in relation to or arising out of the use of the Content.

This article may be used for research, teaching, and private study purposes. Terms & Conditions of access and use can be found at <http://www.tandfonline.com/page/terms-and-conditions>

It is essential that you check the license status of any given Open and Open Select article to confirm conditions of access and use.

Optimisation of interface roughness and coating thickness to maximise coating–substrate adhesion – a failure prediction and reliability assessment modelling

M.H. Nazir^{a*}, Z.A. Khan^a and K. Stokes^b

^aBournemouth University, Sustainable Design Research Centre (SDRC), Faculty of Science and Technology, Bournemouth, BH12 5BB, UK; ^bDefence Science and Technology Laboratory (DSTL), Salisbury, UK

(Received 28 January 2015; accepted 4 March 2015)

A mathematical model for failure prediction and reliability assessment of coating–substrate system is developed based on a multidisciplinary approach. Two models for diffusion and bending of bi-layer cantilever beam have been designed separately based on the concepts of material science and solid mechanics respectively. Then, these two models are integrated to design an equation for debonding driving force under mesomechanics concepts. Mesomechanics seeks to apply the concepts of solid mechanics to microstructural constituent of materials such as coatings. This research takes the concepts of mesomechanics to the next level in order to predict the performance and assess the reliability of coatings based on the measure of debonding driving force. The effects of two parameters i.e. interface roughness and coating thickness on debonding driving force have been analysed using finite difference method. Critical/threshold value of debonding driving force is calculated which defines the point of failure of coating–substrate system and can be used for failure prediction and reliability assessment by defining three conditions of performance i.e. safe, critical and fail. Results reveal that debonding driving force decreases with an increase in interface roughness and coating thickness. However, this is subject to condition that the material properties of coating such as diffusivity should not increase and Young's modulus should not decrease with an increase in the interface roughness and coating thickness. The model is based on the observations recorded from experimentation. These experiments are performed to understand the behaviour of debonding driving force with the variation in interface roughness and coating thickness.

Keywords: coating debondment; blister; delamination; diffusion; bi-layer cantilever; mathematical model; simulation; finite difference method; failure prediction; reliability assessment

Nomenclature

Unless otherwise specified, the following nomenclature is used in this paper.

Notation	Description
u_k	chemical potential of substance k
u_k^s	chemical potential in the given standard state
R	molar gas constant
T	temperature

*Corresponding author: Email: hnazir@bournemouth.ac.uk

© 2015 The Author(s). Published by Taylor & Francis.

This is an Open Access article distributed under the terms of the Creative Commons Attribution-NonCommercial-NoDerivatives License (<http://creativecommons.org/licenses/by-nc-nd/4.0/>), which permits non-commercial re-use, distribution, and reproduction in any medium, provided the original work is properly cited, and is not altered, transformed, or built upon in any way.

a_n	activity of component n
c_k	concentration of substance k
σ_{ij}	stress tensor
n_k	molar concentration of substance k
de_{ij}	strain volume
ε_{ij}	infinitesimal strain tensor
V	volume of element
e_{ij}^k	volumetric strain tensor of diffusing substance k
δ_{ij}	Kronecker delta
e^k	scalar term equal to $\overline{V_{P_k}}$
$\overline{V_{P_k}}$	partial molar volume of substance k
V_{m_k}	molar volume of solution
P	pressure
ρ_k	mass density
m_k	molar mass
$\mu_k^{\hat{O}}$	chemical potential corresponding to the stressed state of the coating
σ_m	average of principle stresses of the stress tensor
σ_i	principle stresses
σ_{d_i}	diffusion induced stresses
$\frac{\sigma_{r_i}}{J_k}$	residual stresses
J_k	diffusion flux of a substance k
D_k	diffusion coefficient of substance k
h	thickness of coating
s	thickness of substrate
x	free surface
l_c	length of coating
ε	diffusion induced strain
ε_u	uniform component
ε_b	bending component
ζ	radius of curvature of coating corresponding diffusion
α	thermal expansion coefficient
M	applied moment
R_a	average interface roughness
L_a	average wavelength of the roughness
λ	interface roughness ($=R_a^2/L_a$)
G	energy release rate
G_{cr}	critical energy release rate
$\partial\sigma_{d_c}/\partial t$	change in diffusion induced stress with time ($=\sigma'_{d_c}$)
σ_{cr}	critical stress when the coating just begins to debond
\cap	debonding index ($=\sigma'_{d_c}/\sigma_{cr}$)
\cap_{cr}	critical debonding index
j	mode-mix function
Γ_{IC}	mode I toughness
F	debonding driving force
χ	Dundur's elastic mismatch
ω	angular deflection parameter dependent upon Dundur's elastic mismatch
ψ	mode adjustment term
\mathbb{H}	deflection index parameter

1. Introduction

Coatings or paints tend to prevent the effects of physical and chemical attack on the substrate. However, when the coated or painted structures are subjected to short-term or long-term chemical effect, the first form of failure is often debondment of the coating layer from substrate.[1] This functional failure of the coating may ultimately lead to structural failure, if not properly treated at right time. The functionality and reliability of coating–substrate systems, which are subjected to chemical effects, are strongly related to chemical stresses (or diffusion-induced stresses) of coatings. The diffusion-induced stress builds up in the coating on the substrate due to the chemical absorption,[2] adsorption [3] or mass change.[4] The evolution of diffusion-induced stress in the coating results in the debondment of coating from the substrate.

The debondment of coating has drawn a considerable interest in the recent decades.[5,6] However, most of the research is based on the effects of residual stresses due to thermal expansion mismatch, and their effect on coating–substrate adhesion.[7–10] The evolution of diffusion-induced stresses in coatings was originally analysed by Podstrigach and Shevchuk [11]. Since then, some researchers [12–17] had made a series of studies of diffusion-induced stresses in coatings and had come up with experiments and numerical models to analyse coating–substrate debondment. Also, in recent research work, models for coating–substrate debondment involving diffusion-induced stresses, developed by Nguyen et al. [18], Prawoto et al. [19,20], Cui et al. [21], Yang and Li [22] and Rusanov [23] are based on various numerical methods and techniques. It is worth noting that the occurrence of residual stress in coating–substrate systems due to thermal expansion mismatch is unavoidable in practice. However, for the purpose of study, the effects of residual stresses on coating–substrate debondment are neglected. Only the diffusion coefficient and the concentration of solvent atoms will be enhanced by the hydrostatic stress according to Wang et al. [24] and Yang and Li [22].

Actually, the diffusion-induced stress depends on Fick's law and thermodynamic properties of coating–substrate system which comes under the discipline of material science. The diffusion-induced stress directly affects the bending of coating which results in debondment.[25] The propagation of debondment at the coating–substrate interface is based on the concepts of bi-layer cantilever beam. The concepts of bi-layer cantilever beam come under the discipline of solid mechanics. The coupling of material science and solid mechanics concepts forms a basis of mesomechanics.[26–28] Mesomechanics seeks to apply mechanics concepts to the microstructural constituents of materials which can be used to predict the coating–substrate adhesion failure based on the measure of debonding driving force. Debonding driving force under mesomechanics is the key element which influences the coating–substrate adhesion. Higher debonding driving force accounts for lower interface adhesion and vice versa. This coupling of two distinct disciplines to predict the failure and analyse the performance of coating–substrate system based on the measure of debonding driving force has not been involved in the existing studies. This will deserve a higher degree of accuracy of the prediction model. It is therefore, essential to predict the failure and analyse the performance of coating–substrate system in consideration of the coupling of diffusion and bi-layer cantilever beam concepts.

This work is the continuation of research within our group.[28–31] The purpose of this investigation is to predict the adhesion failure and assess the reliability of coating–substrate system using the principles of debondment of the bi-layered cantilever induced by diffusion. For this purpose, two most important parameters that influence

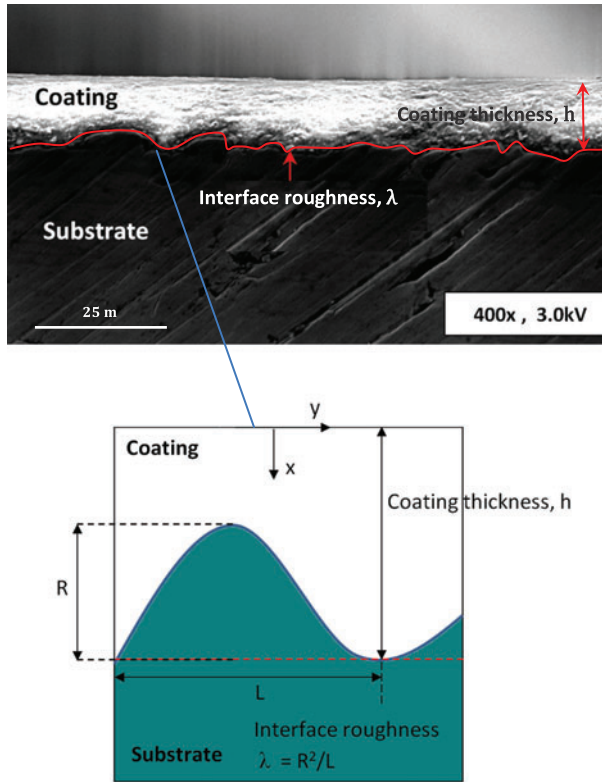


Figure 1. Cross sectional SEM of undulating nature of coating–substrate interface (roughness) and coating thickness in a spray coating system (above) and schematic of coating–substrate interface roughness and coating thickness (below).

the adhesion in terms of debonding driving force are used for investigation.[32–35] These parameters are interface roughness of coating–substrate and coating thickness as shown in Figure 1. The investigation has been performed using a ‘two set-up approach’: (i) set-up 1: constant coating thickness with variable interface roughness and (ii) set-up 2: constant interface roughness with variable coating thickness. At first, the experimental study is performed and the samples for the two set-ups are prepared accordingly. These experiments are performed using the samples prepared for two set-ups. The experiments involve Vickers indentation test and ASTM-B117 test. These experiments are performed to understand the behaviour of debonding driving force with the variation in interface roughness and coating thickness under two set-ups, respectively. Comparison of the values of debonding driving force for various values of interface roughness and coating thickness are used to find the critical/threshold in terms of debonding driving force. This critical/threshold defines the point of failure.

After understanding the complete behaviour of debonding driving force using experimentation, a mathematical model for failure prediction is developed. Two independent mathematical models are developed for diffusion and bi-layer cantilever beam under material science and solid mechanics disciplines, respectively. These two models are then integrated to develop an equation for debonding driving force under mesomechanics. This equation is further modified to find the critical/threshold value of debonding driving force which defines the failure point of coating–substrate adhesion. An

algorithm is developed based on finite difference method in order to simulate the timely variation of debonding driving force due to change in interface roughness and coating thickness. Further, critical/threshold points are defined on these simulated graphs which characterise three conditions of coating–substrate performance i.e. safe, critical and fail. At the end, a model for the assessment of reliability of coating–substrate system is developed by utilising the above developed failure prediction model.

2. Experimental set-up and observations

AISI 1010 Carbon Steel is used as a substrate and primer (red-oxide) is used as a coating in this paper. The primer is sprayed using conventional spraying gun. The experimental design has been divided into the following two set-ups to analyse the effect of interface roughness λ and coating thickness h on debonding driving force F ,

- (i) Set-up 1: constant coating thickness h with variable interface roughness λ .
- (ii) Set-up 2: constant interface roughness λ with variable coating thickness h .

2.1. Samples preparation for set-up 1-with variable interface roughness λ

Set-up 1 is designed to analyse the effect of various values of interface roughness λ on debonding driving force F while keeping the coating thickness h constant for all the samples. Ten samples were prepared with interface roughness (μm): λ I = 0.4, λ II = 1.1, λ III = 2.4, λ IV = 4.1, λ V = 5.3, λ VI = 6.8, λ VII = 7.5, λ VIII = 8.6, λ IX = 9.4 and λ X = 10.6, respectively. All the samples had a constant coating thickness $h = 30 \mu\text{m}$. The values of interface roughness λ are measured using three-dimensional scanning interferometry.[36] These roughness values are averaged through 10 data points per sample.

2.2. Samples preparation for set-up 2-with variable coating thickness h

Set-up 2 is designed to analyse the effect of various values of coating thickness h on the debonding driving force F while keeping the interface roughness λ constant for all samples. Ten samples were prepared with coating thicknesses (μm): h I = 10.8, h II = 14.6, h III = 18.5, h IV = 22.4, h V = 26.2, h VI = 30.1, h VII = 34, h VIII = 37.8, h IX = 41.7 and h X = 45.6, respectively. All the samples had a constant interface roughness $\lambda = 5.3 \mu\text{m}$. Like roughness, the values of coating thickness h are measured using three-dimensional scanning interferometry. These thickness values for the coatings are averaged through 10 data points per sample.

One important thing that was highly considered during sample preparation was that material properties of coating such as diffusivity and Young's modulus should be constant for all the samples. Increase in diffusivity makes coating more permeable to diffusing component and decrease in Young's modulus increases the flexibility of coating. Both the changes can significantly affect the results of debonding driving force. Diffusivity and Young's modulus of coating depends on material's microstructure.[37,38]

2.3. Experimental observations

2.3.1. Vickers indentation test of samples

Debonding driving force F for the samples under each set-up (1 and 2) was calculated by deploying an artificial method of debonding i.e. Vickers indentation. Debonding

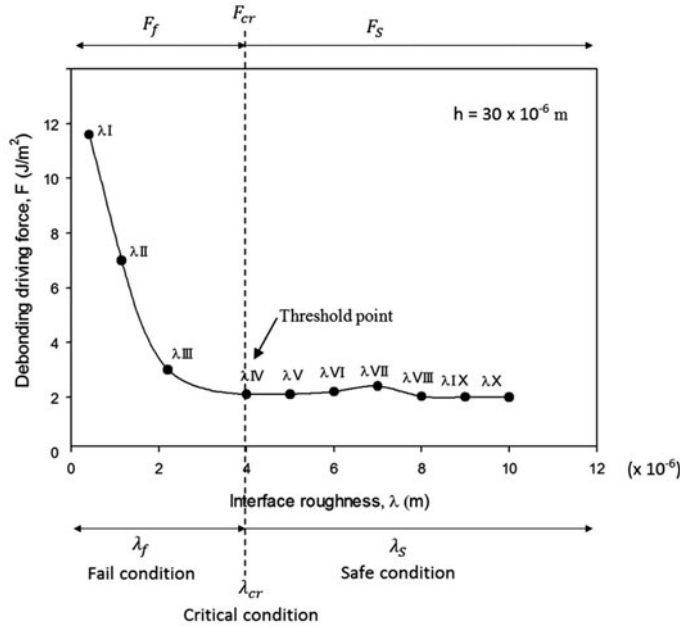


Figure 2(a). *Experimental observation using set-up 1*: Debonding driving force as a function of interface roughness λ keeping constant value of coating thickness h . Graph in figure also defines safe, critical and fail conditions for coating performance.

driving force F of samples was calculated before the samples were subjected to ASTM-B117 environmental test.

Debonding driving force F of samples for set-up 1 is shown in Figure 2(a). The graph indicates that the debonding driving force F decreases with an increase in interface roughness and becomes stable. The critical value of debonding driving force i.e. F_{cr} corresponding to critical interface roughness λ_{cr} indicates the threshold point on graph. This threshold is the incipient requirement for the debondment initiation. If the value of F corresponding to λ exceeds this threshold point, then this results in the debondment of coating from the substrate (fail condition). Conversely, if the value of F corresponding to λ is less than the threshold point, then the coating remains intact with the substrate (safe condition). Sample with interface roughness (μm) λ IV = 4.1 is treated as *critical*. Samples with interface roughness (μm) λ I = 0.4, λ II = 1.1, λ III = 2.4 are treated as *fail*. Samples with interface roughness (μm) λ V = 5.3, λ VI = 6.8, λ VII = 7.5, λ VIII = 8.6, λ IX = 9.4 and λ X = 10.6 are treated as *safe*.

Debonding driving force F of samples for set-up 2 is shown in Figure 2(b). The graph indicates an exponential decay of debonding driving force F with an increase in coating thickness h . The critical value of debonding driving force i.e. F_{cr} corresponding to critical coating thickness h_{cr} indicates the threshold point on graph. For set-up 2, sample with coating thickness (μm) h VII = 34 is treated as *critical*. Samples with coating thicknesses (μm) h I = 10.8, h II = 14.6, h III = 18.5, h IV = 22.4, h V = 26.2, h VI = 30.1 are treated as *fail*. Samples with coating thicknesses (μm) h VIII = 37.8, h IX = 41.7 and h X = 45.6 are treated as *safe*.

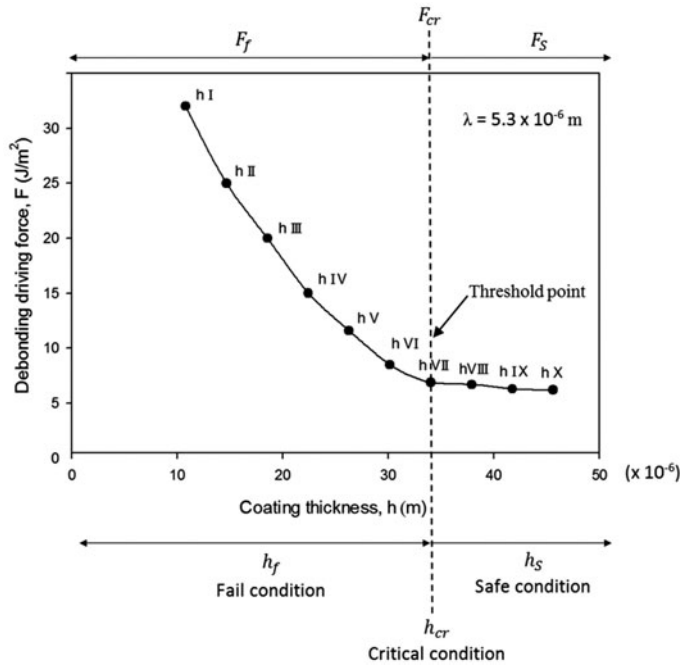


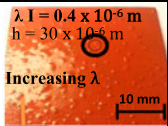
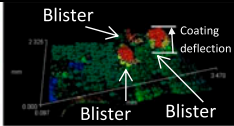
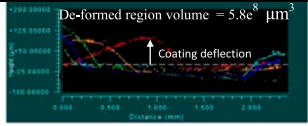
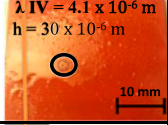
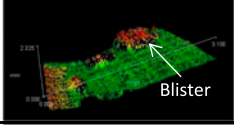
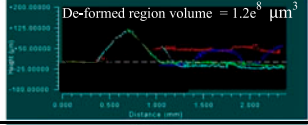
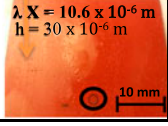
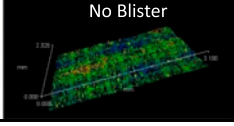
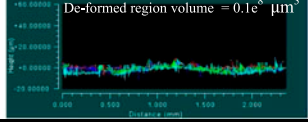
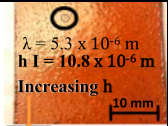
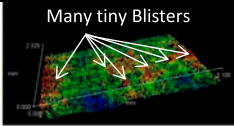
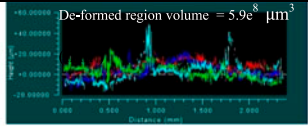
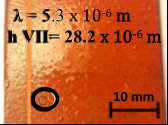
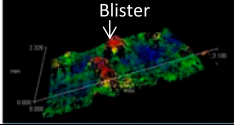
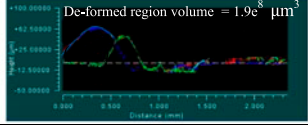
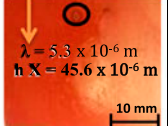
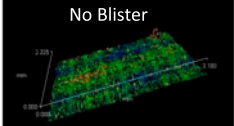
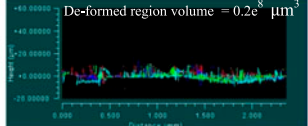
Figure 2(b). *Experimental observation using set-up 2: Debonding driving force as a function of coating thickness h keeping constant value of interface roughness λ . Graph in figure also defines safe, critical and fail conditions for coating performance.*

2.3.2. ASTM-B117 test of samples

ASTM-B117 environmental test was employed to analyse the debondment of coating under simulated environmental condition. This test was performed to investigate the performance of coating under the effect of saline fog at temperature $T = 35\text{ }^{\circ}\text{C}$. This test makes use of sodium chloride which acts as a diffusing substance through coating. The same samples which were analysed using indentation were now subjected to environmental test. This exposure of samples to ASTM-B117 test gave rise to blisters on coating due to diffusing substance which results in coating debondment. The evaluation of these blisters was performed by using interferometry. The interferometry was used for three-dimensional mapping and volume measurement of blisters (within circled area) as shown in Table 1. Along with interferometry, ASTM-D714 was also used to evaluate the degree of blistering using photographic references of samples. Post ASTM-B117 test results showed that the samples with maximum interface roughness and coating thickness exhibit maximum resistance to coating failure and vice versa. Three samples from each set-up (1 and 2) under safe, critical and fail conditions are shown in Table 1 with three colours (green-safe, yellow-critical and red-fail).

Next sections explain the development of a mathematical model based on the observations made from experimentation.

Table 1. Three samples from each set-up (1 and 2) under safe, critical and fail conditions. The interferometry was used for 3-D mapping and volume measurement of blisters (within circled area). ASTM-D714 was also used to evaluate the degree of blistering using photographic references of samples.

Sample	Samples photographs	3-D mapping of black circled area on sample image	Surface profiling for upward (deflection) volume calculation	ASTM D-714 blister evaluation
Setup 1 Variable interfacial roughness, λ				
Fail condition λ I	λ I = 0.4×10^{-6} m $h = 30 \times 10^{-6}$ m Increasing λ 		 De-formed region volume = $5.8e^8 \mu\text{m}^3$	Dense blisters
Critical condition λ IV	λ IV = 4.1×10^{-6} m $h = 30 \times 10^{-6}$ m 		 De-formed region volume = $1.2e^8 \mu\text{m}^3$	Few blisters
Safe condition λ X	λ X = 10.6×10^{-6} m $h = 30 \times 10^{-6}$ m 		 De-formed region volume = $0.1e^8 \mu\text{m}^3$	No blisters
Setup 2 Variable coating thickness, h				
Fail condition h I	$\lambda = 5.3 \times 10^{-6}$ m h I = 10.8×10^{-6} m Increasing h 		 De-formed region volume = $5.9e^8 \mu\text{m}^3$	Dense blisters
Critical condition h VII	$\lambda = 5.3 \times 10^{-6}$ m h VII = 28.2×10^{-6} m 		 De-formed region volume = $1.9e^8 \mu\text{m}^3$	Few blisters
Safe condition h X	$\lambda = 5.3 \times 10^{-6}$ m h X = 45.6×10^{-6} m 		 De-formed region volume = $0.2e^8 \mu\text{m}^3$	No blisters

3. Modelling methodology

The debondment of coating from the substrate is a multidisciplinary problem. It needs to be investigated from multi-dimensions by fostering a close collaboration between material science and solid mechanics disciplines. Mesomechanics seeks to imply the principles of solid mechanics to microstructural constituent of materials such as coatings. This research takes the concepts of mesomechanics to the next level in order to predict the failure and analyse the service life of coatings bonded to the substrate. The developed model follows the methodology given in Figure 3.

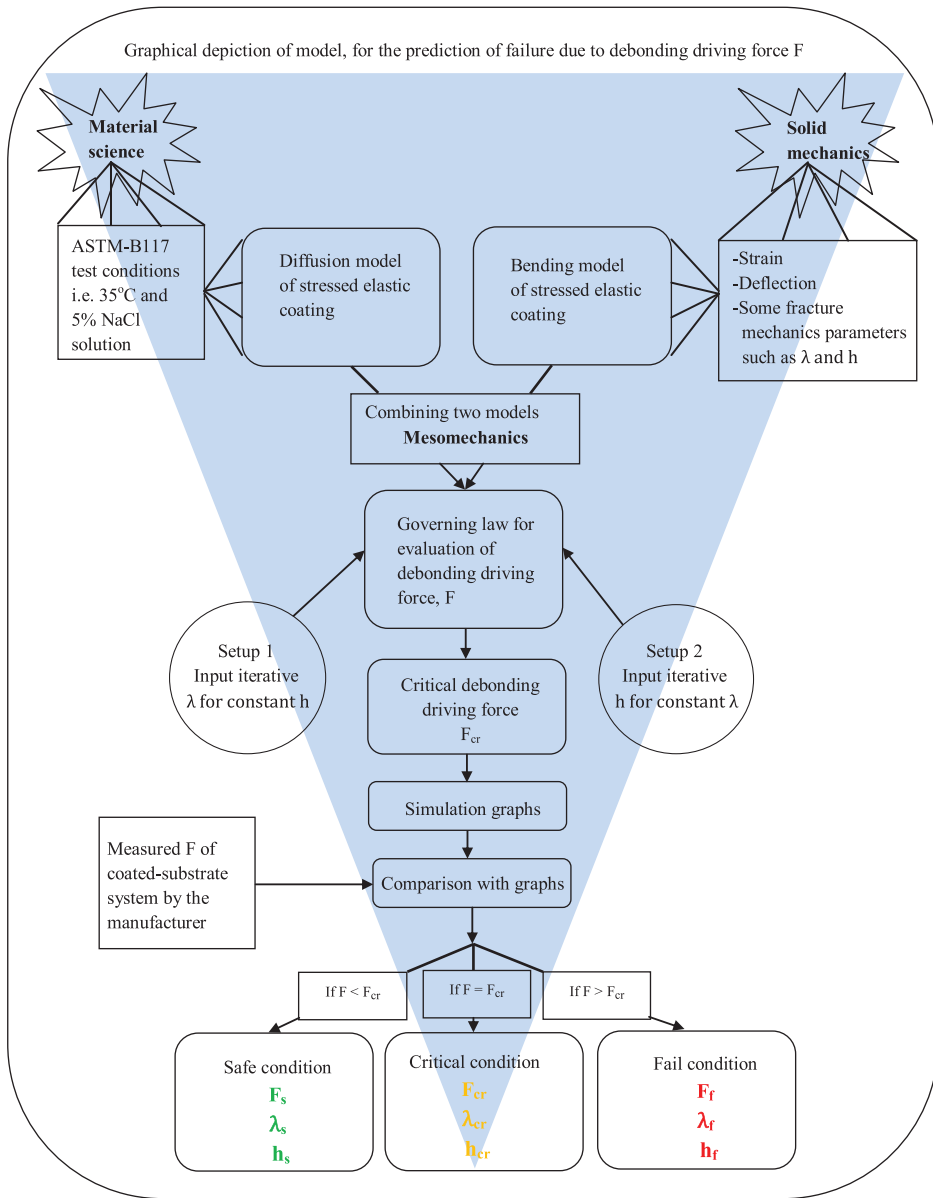


Figure 3. Graphical depiction of the design for mathematical model for prediction of failure (modelling methodology).

The design methodology follows the top-down approach. At the top of hierarchy, are the two major disciplines i.e. material science and solid mechanics. Each discipline encapsulates its constituent parameters, respectively. These parameters describe the mechanism of coating debondment. Temperature T ($=35^\circ\text{C}$) and percentage NaCl concentration ($=5\%$ NaCl solution) for ASTM-B117 test are described as constituent parameters forming material science. While strain, deflection of coating and some fracture mechanics parameters such as λ and h are described as constituent parameters

forming solid mechanics. These respective constituent parameters of material science and solid mechanics are used for the development of diffusion model and bending model of stressed elastic coatings, respectively. The equations for both the approaches (diffusion and bending) are designed separately and then fused to form a governing law for the evaluation of debonding driving force F . The fusion of two distinct approaches (diffusion and bending) forms a basis of mesomechanics as shown in Figure 3. The debonding driving force F under mesomechanics is the key element responsible for the coating debondment.

Based on the numerical simulations with the finite difference method, the effect of interface roughness λ (set-up 1) and coating thickness h (set-up 2) on debonding driving force F is analysed. Critical/threshold points are calculated which are then defined on these simulation graphs. The simulation graphs along with critical/threshold points define the three conditions of coating performance based on the value of debonding driving force i.e. safe, critical and fail. The graphs which are generated using simulations can be used by the manufacturer at the time of manufacturing to design for durability by identifying that under which condition their manufactured coating–substrate system lies. These graphs can also be used to evaluate the performance of coatings in test conditions such as indentation test or ASTM-B117. Next section will focus on the design of mathematical model for failure prediction of coating–substrate system based on the above methodology.

4. Mathematical model (a failure prediction model)

4.1. Diffusion model of stressed elastic coating – application of material science concepts

Thermodynamics and diffusion mechanism are the potential research topics in material science discipline. This part of modelling is specifically developed by considering the diffusion of substance k such as salt solution when the primer-coated steel sample is exposed to ASTM-B117 test condition i.e. $T = 35^\circ\text{C}$ and 5% NaCl solution. The diffusing component n of a substance k maintains a concentration c_n over an entire exposed surface of the coating as shown in Figure 4.

The theory of irreversible thermodynamics states that the change in thermodynamics state of a system due to the loss or gain of a particle defines the chemical potential of the components.[39] The chemical potential u_k of substance k can be expressed as [40]:

$$u_k = u_k^s + RT \ln(a_n) \quad (1)$$

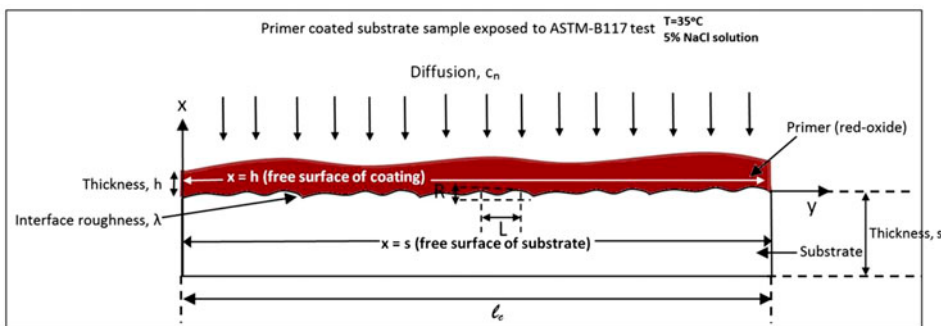


Figure 4. A schematic of coating–substrate system representation in terms of bi-layer cantilever beam.

where R is the molar gas constant; T is the temperature; u_k^s is the chemical potential in the given standard state; a_n is the activity of component n which is equivalent to the concentration c_k of a substance subject to the condition of infinitely dilute solutions.

When the thin elastic coating (primer) is subjected to a highly alkaline environment such as ASTM-B117 test, then the diffusion-induced stress tends to develop compound stress fields. For such case, the change in stress is coupled with the change in chemical potential and can be represented in the form of Maxwell relation as [41]:

$$\frac{\partial u_k}{\partial \sigma_{ij}} = -\frac{\partial e_{ij}}{\partial n_k} = -e_{ij}^k \quad (2)$$

where σ_{ij} is the stress tensor; n_k is the molar concentration of diffusing substance k ; $de_{ij} = V de_{ij}$ represents the strain volume and shows the relationship between infinitesimal strain tensor ε_{ij} ($ij = 1, 2, 3$) and volume of element V ; e_{ij}^k is the volumetric strain tensor of diffusing substance k considering an isotropic strain volume,[42] that is,

$$e_{ij}^k = e^k \frac{\delta_{ij}}{3} \quad (3)$$

where δ_{ij} is the Kronecker delta; e^k is the scalar term and can be treated as being equivalent to the partial molar volume \overline{V}_{P_k} of diffusing substance k i.e. $e^k = \overline{V}_{P_k}$. \overline{V}_{P_k} can be found using Euler's first theorem for homogeneous functions [43] as,

$$\overline{V}_{P_k} = \left(\frac{\partial V_{m_k}}{\partial n_k} \right)_{T,P,n_{k \neq i}} = \left(\frac{V_{m_{k_2}} - V_{m_{k_1}}}{n_{k_2} - n_{k_1}} \right)_{T,P,n_{k \neq i}} \quad (4)$$

where \overline{V}_{P_k} depends on the molar volume of solution V_{m_k} , where V_{m_k} denotes a generic extensive property of a solution which depends on temperature T , pressure P and molar concentration of diffusing substance k i.e. n_k .

Consider one mole change in concentration n_k from n_{k_1} to n_{k_2} keeping temperature T and pressure P constant. For such a case, $V_{m_{k_2}} - V_{m_{k_1}}$ is the change in molar volume associated with per molar change in concentration of a diffusing substance k from n_{k_1} to n_{k_2} . The molar volumes at two different stages of change are calculated using a well-known mass density relation as:

$$V_{m_{k_2}} = \frac{m_{k_2}}{\rho_{k_2}}, V_{m_{k_1}} = \frac{m_{k_1}}{\rho_{k_1}} \quad (5)$$

where m_{k_2} , m_{k_1} and ρ_{k_2} , ρ_{k_1} denote the molar masses and mass densities, respectively, at two different stages of change.

For the case of an isotropic solution, Equation (2) can be integrated in conjunction with Equations (3)–(5),

$$u_k^Q = u_k - \int_0^{\sigma_{ij}} e_{ij} \, d\sigma_{ij} = u_k - \int_0^{\sigma_m} \overline{V}_{P_k} \, d\sigma_m \quad (6)$$

Substituting u_k from Equation (1) into Equation (6) gives,

$$u_k^Q = u_k^s + RT \ln(c_k) - \int_0^{\sigma_m} \overline{V}_{P_k} \, d\sigma_m \quad (7)$$

where u_k^Q represents the chemical potential corresponding to the stressed state of the coating; $\sigma_m = \frac{1}{3} \sum_{i=1}^3 \sigma_i$ is the average of the three principle stresses of the stress tensor and σ_i are the principle stresses.

The deformation of linear elastic ‘porous’ coating due to the coupling between the linear diffusion of a substance k and the stress tensors is defined by linear poroelasticity theory.[44,45] This theory states that the infinitely slower atomic diffusion of a substance k compared to the deformation of stressed elastic coating will equilibrate the mechanical properties of coating much faster than that of diffusion. The concepts of linear poroelasticity can be used in conjunction with the formal theory of linear elasticity to model the current problem. Therefore, the principle stresses σ_i can be written as a sum of diffusion induced stresses σ_{d_i} and residual stresses σ_{r_i} i.e. $\sigma_i = \sigma_{d_i} + \sigma_{r_i}$.

It is possible to minimise the effect of residual stress σ_{r_i} using specified temperature gradients and controlled phase transformations,[46–50] therefore, $\sigma_{r_i} \approx 0$. Accordingly, σ_m can be modified in terms of diffusion induced stress as:

$$\sigma_m = \frac{1}{3} \sum_{i=1}^{i=3} (\sigma_i) = \frac{1}{3} \sum_{i=1}^{i=3} (\sigma_{d_i} + \sigma_{r_i}) = \sigma_d \quad (8)$$

Substituting Equation (8) in Equation (7) gives the chemical potential u_k^O of a diffusing substance k in the stressed coating which is dependent on a scalar ($\overline{V_{P_k}}$) and a tensor (σ_d) as:

$$u_k^O = u_k^s + RT \ln(c_k) - \overline{V_{P_k}} \sigma_d \quad (9)$$

where $\overline{V_{P_k}}$ is a scalar term and does not include the effect of stress tensor.

Consider the case of an inhomogeneous distribution of solute particles in a non-ideal solution. The driving force for the diffusion of substance k is the gradient of chemical potential $-\nabla u$ of that substance. Fick’s first law of diffusion relates the diffusion flux \vec{J}_k of a substance k with the gradient of chemical potential as:

$$\vec{J}_k = -\frac{D_k c_k}{RT} \nabla u_k^O \quad (10)$$

The vector form of diffusion flux \vec{J}_k is directly proportional to the gradient of chemical potential [51]; D_k is the diffusion coefficient of substance k in the stress-free isotropic coating.

Substituting Equation (9) in Equation (10) gives the diffusion flux \vec{J}_k of diffusing substance k in the stressed coating as:

$$\vec{J}_k = -D_k \nabla c_k + \frac{D_k c_k \overline{V_{P_k}}}{RT} \nabla \sigma_d \quad (11)$$

The concentration of a substance k within the stressed coating changes with time. Fick’s second law of diffusion in conjunction with the law of conservation of mass can be applied as:

$$\nabla \cdot \vec{J}_k = -\frac{\partial c_k}{\partial t} \quad (12)$$

Multiplying both sides of Equation (11) with the gradient operator ∇ and then substituting Equation (11) in Equation (12). This gives the differential equation which includes the effect of diffusion induced stress as:

$$\frac{\partial c_k}{\partial t} = D_k \nabla^2 c_k - \frac{D_k \overline{V_{P_k}}}{RT} \nabla c_k \cdot \nabla \sigma_d - \frac{D_k \overline{V_{P_k}}}{RT} c_k \cdot \nabla^2 \sigma_d \quad (13)$$

Equation (13) follows the law of conservation of mass, as the change of concentration of diffusing substance k with time $\frac{\partial c_k}{\partial t}$ on the left side of Equation (13) must be equal to the local decrease of the diffusion flux and other two stress-assisted terms on right side of equation.

4.2. Bending model of bi-layered cantilever – application of solid mechanics concepts

This part of modelling is specifically designed based on the concepts of solid mechanics incorporating the principles of bi-layer cantilever beam. According to the current design, one adherend of the bi-layer cantilever beam acts as coating, while the other adherend acts as substrate. The interface between the coating and substrate is located at $x = 0$ along the coordinate axis; the free surface of the coating and the substrate is located at $x = h$ and $x = -s$, respectively, as shown in Figure 4. It is worth nothing that for the case which is reported in this research is based on the fact that only one layer of cantilever which is the coating, exhibits bending. The reason is that the thickness of coating is much less than the thickness of substrate.

The analysis in this paper is based on the following assumptions: (i) coating thickness h is very small compared to substrate thickness s , (ii) coating thickness h is strictly small compared to its length l_c i.e. $(h/l_c) < 1$ as shown in Figure 4, (iii) coating and substrate materials are homogeneous, isotropic, linearly elastic and other parameters such as Young's modulus, diffusivity and chemical potential are invariable during debonding and diffusion and (iv) the strain tensor along with principle strains is extremely small.

The analyses of the bending of bi-layer cantilever beam follow the assumption that the diffusion-induced stress σ_d is initially zero at time $t = 0$. After the incubation of diffusive substance k in both layers of cantilever beam at time $t > 0$, the layer which represents the coating, will start to bend and the diffusion-induced stress will therefore, appear.

According to Hsueh [50], the strain distribution in a system (diffusion induced strain) ε can be decomposed into a uniform component ε_u and a bending component ε_b as:

$$\varepsilon = \varepsilon_u + \varepsilon_b = \varepsilon_u + \frac{x - t_b}{\zeta} \quad (\text{for } -s \leq x \leq h) \quad (14)$$

$x = t_b$ represents the neutral point of the bending axis in a coordinate system where bending strain component ε_b is zero; ζ represents the radius of curvature corresponding to diffusion. The analyses of strain distribution (Equation (14)) at the interface of coating and substrate comply with the strain continuity equation in Timoshenko shear model.[52]

The normal stresses in cantilever are related to thermal strain using stress–strain relation as [50]:

$$\sigma = E(\varepsilon - \alpha\Delta T) \quad (15)$$

where $\alpha\Delta T$ dictates the thermal strain with α representing the thermal expansion coefficient and ΔT representing the change in temperature. For diffusion processes, the coating properties may be assumed to change linearly [53] with the concentration of diffusing substance k , which results in diffusion-induced stresses. Therefore, it is possible to calculate diffusion-induced stress by analogy to thermal stress. Prussin [54] and Zhang et al. [55], previously treated concentration gradients c'_k analogously to those generated by temperature gradients ΔT and partial molar volume \bar{V}_{P_k} analogous to thermal expansion α . Therefore, Equation (15) can be modified to obtain the expressions for normal stresses in coating and substrate as:

$$\sigma_{d_c} = E_c \left(\varepsilon - \frac{1}{3} c'_{k_c} \overline{V_{P_{k_c}}} \right) \quad (16a)$$

$$\sigma_{d_s} = E_s \left(\varepsilon - \frac{1}{3} c'_{k_s} \overline{V_{P_{k_s}}} \right) \quad (16b)$$

$c'_{k_i} = c_{k_i} - c_{k_o}$ is treated as the concentration change of the diffusing substance k from the original (stress-free) value where $i = c, s$. For the condition when the system has planar geometry rather than a linear geometry, then the bi-axial strains are identical along y and z plane, therefore, E_i can be replaced by $E_i/(1 - \nu_i)$, where ν_i is the Poisson's ratio.

Consider the 'average stress distribution' through both the layers of cantilever. The average diffusion-induced stress through coating and substrate can be defined by incorporating Equations (16a) and (16b) as:

$$\sigma_{d_c} = \int_{Z_c} \sigma_{d_c} dZ_c = \int_{Z_c} E_c \left(\varepsilon - \frac{1}{3} c'_{k_c} \overline{V_{P_{k_c}}} \right) dZ_c \quad (17a)$$

$$\sigma_{d_s} = \int_{Z_s} \sigma_{d_s} dZ_s = \int_{Z_s} E_s \left(\varepsilon - \frac{1}{3} c'_{k_s} \overline{V_{P_{k_s}}} \right) dZ_s \quad (17b)$$

where $Z_c = b_n$, $Z_s = b_s$ and $b = b_s = b_n$. The strain and stress distribution in bi-layer cantilever beam (Equations (14), (17a) and (17b)) are dependent on the solution of two parameters i.e. ε_u and ζ . It is possible to find ε_u and ζ by using the following two boundary conditions.

At first, the resultant force due to uniform stress component is zero, such that

$$\int_{Z_c} E_c \left(\varepsilon_u - \frac{1}{3} c'_{k_c} \overline{V_{P_{k_c}}} \right) dZ_c + \int_{Z_s} E_s \left(\varepsilon_u - \frac{1}{3} c'_{k_s} \overline{V_{P_{k_s}}} \right) dZ_s = 0 \quad (18)$$

ε_u is determined by the solution of Equation (18),

$$\varepsilon_u = \frac{1}{3} \left(\frac{E_c h \overline{V_{P_{k_c}}} c'_{k_s} + E_s s \overline{V_{P_{k_s}}} c'_{k_c}}{E_c h + E_s s} \right) \quad (19)$$

where $\overline{c'_{k_c}} = \frac{1}{h} \int_0^h c'_{k_c} dx$ and $\overline{c'_{k_s}} = \frac{1}{s} \int_{-s}^0 c'_{k_s} dx$.

Second, the bending moment of cantilever layers with respect to neutral point of bending axis i.e. $x = t_b$ is zero, such that

$$\int_{Z_c} \sigma_{d_c} (x - t_b) dZ_c + \int_{Z_s} \sigma_{d_s} (x - t_b) dZ_s = 0 \quad (20)$$

The bending curvature of cantilever $1/\zeta$ can be determined from the solution of Equations (14), (17a), (17b), (19) and (20) as,

$$\frac{1}{\zeta} = \frac{2 \left[(E_c \overline{V_{P_{k_c}}} M_c + E_s \overline{V_{P_{k_s}}} M_s) - (E_c \overline{V_{P_{k_c}}} h \overline{c'_{k_c}} + E_s \overline{V_{P_{k_s}}} s \overline{c'_{k_s}}) t_b \right]}{E_c h^2 (2h - 3t_b) + E_s s^2 (2s + 3t_b)} \quad (21)$$

where M is the applied moment such that $M_c = \frac{1}{h} \int_0^h c'_{k_c} x dx$ and $M_s = \frac{1}{s} \int_{-s}^0 c'_{k_s} x dx$.

When the concentration of diffusing substance k is distributed in a uniform pattern along both the layers of cantilever than, Equation (21) can be modified as:

$$\frac{1}{\zeta} = \frac{2 \left[E_c E_s h s (2s) \left(\overline{V_{P_{kc}}} c'_{k_c} - \overline{V_{P_{ks}}} c'_{k_s} \right) \right]}{E_c^2 h^4 + E_s^2 s^4 + 2 E_c E_s h s (2h^2 + 3hs + 2s^2)} \quad (22)$$

When the first-order approximation is taken, Equation (22) becomes,

$$\frac{1}{\zeta} = \left(\frac{E_c}{E_s h} \right) \left(1 - \frac{4E_c h}{E_s s} \right) \left(\overline{V_{P_{kc}}} c'_{k_c} - \overline{V_{P_{ks}}} c'_{k_s} \right) \quad (23)$$

The above equations (22 and 23) which are derived for the bending of bi-layer cantilever due to diffusion of substance k are analogous to equations derived by Hsueh [50] for thermal stresses when term $\overline{V_{P_{kc}}} c'_{k_c} - \overline{V_{P_{ks}}} c'_{k_s}$ is replaced by $(\alpha_c - \alpha_s) \Delta T$. The equations are also analogous to equations derived by Xuan et al. [56] for deformation of thin sensor films.

4.3. Combined model (diffusion and bending models) – mesomechanics approach

This part of modelling gives a holistic design based on diffusion and bending models. The stitching of both the components together and incorporating fracture mechanics concepts form the mesomechanics approach. This approach is further utilised to predict the coating failure. The modelling of this part follows the following assumptions: (i) average interface roughness R_a is less than the average wavelength of the roughness L_a at the interface i.e. $(\lambda = R_a^2/L_a) < 1$ as shown in Figure 4, (ii) the frictional sliding plays a negligible role, (iii) the steady-state energy release rate G of the crack when its length r is far greater than coating thickness h is given by $G = G_{cr}$; where G_{cr} is the critical energy release rate.

Substituting the diffusion-induced stresses, which has been derived in Equation (16a) and (16b) into Equation (13). This forms a coupling relationship between bending of cantilever layers and concentration of diffusing substance k .

$$\frac{\partial c'_{k_c}}{\partial t} = D_{k_c} \left(1 + A_c c'_{k_c} \right) \frac{\partial^2 c'_{k_c}}{\partial x^2} + D_{k_c} A_c \left(\frac{\partial c'_{k_c}}{\partial x} \right)^2 - \frac{D_{k_c} E_c \overline{V_{P_{kc}}}}{RT \zeta} \frac{\partial c'_{k_c}}{\partial x} \quad (24a)$$

$$\frac{\partial c'_{k_s}}{\partial t} = D_{k_s} \left(1 + A_s c'_{k_s} \right) \frac{\partial^2 c'_{k_s}}{\partial x^2} + D_{k_s} A_s \left(\frac{\partial c'_{k_s}}{\partial x} \right)^2 - \frac{D_{k_s} E_s \overline{V_{P_{ks}}}}{RT \zeta} \frac{\partial c'_{k_s}}{\partial x} \quad (24b)$$

In equations, $A_i = \frac{E_i \overline{V_{P_{ki}}}}{RT}$; where $i = c, s$. In the third part on right-hand side of Equation (24a) and (24b), the terms $\frac{E_i}{\zeta}$ can be written as: $\frac{E_c}{\zeta} = \frac{\partial \sigma_{dc}}{\partial t}$ and $\frac{E_s}{\zeta} = \frac{\partial \sigma_{ds}}{\partial t}$.

The current research focuses on the deformation of coatings due to diffusing substance k . Therefore, Equation (24a) can be modified to calculate the change in diffusion-induced stress with time $\frac{\partial \sigma_{dc}}{\partial t}$ due to the change in concentration of diffusing substance k with time $\frac{\partial c'_{k_c}}{\partial t}$, such that,

$$\sigma'_{dc} = \frac{\partial \sigma_{dc}}{\partial t} = \frac{RT \left(1 + A_c c'_{k_c} \right) \left(\frac{\partial^2 c'_{k_c}}{\partial x^2} \right) + RT A_c \left(\frac{\partial c'_{k_c}}{\partial x} \right)^2 - \frac{RT}{D_{k_c}} \frac{\partial c'_{k_c}}{\partial t}}{\overline{V_{P_{kc}}} \left(\frac{\partial c'_{k_c}}{\partial x} \right)} \quad (25)$$

The diffusion-induced stress, which is derived in Equation (25), can be employed to calculate the effect of stresses near crack tips. These crack tips can reside near the

regions of defects in coatings which can incubate the process of debonding. The conventional form of debonding index, as defined by Hutchinson [57–59] is,

$$\Omega = \frac{\sigma'_{dc}}{\sigma_{cr}} = \frac{(1 - \nu^2)}{E} (\sigma'_{dc}) \left(\frac{r}{h}\right)^2 \quad (26)$$

where r is the length of debonding region on the interface between coating and substrate; σ_{cr} is the critical stress when the coating just begins to debond from the substrate in both plane strain and an axis symmetric mode.

Substituting Equation (25) into Equation (26) gives the modified equation, such that,

$$\Omega = \frac{\sigma'_{dc}}{\sigma_{cr}} = \left(\frac{1 - \nu^2}{E}\right) \frac{RT \left(1 + A_c c'_{kc}\right) \left(\frac{\partial^2 c'_{kc}}{\partial x^2}\right) + RT A_c \left(\frac{\partial c'_{kc}}{\partial x}\right)^2 - \frac{RT}{D_{kc}} \frac{\partial c'_{kc}}{\partial t}}{\bar{V}_{P_{kc}} \left(\frac{\partial c'_{kc}}{\partial x}\right)} \left(\frac{r}{h}\right)^2 \quad (27)$$

For the coating debondment to initiate, the value of Ω must exceed a critical value Ω_{cr} . For the plane strain debonding problem, $\Omega_{cr} = 1$.

Griffith and Irwin's employed an energy balance approach [60,61] which was redefined by Hutchinson et al. [58] to investigate failure mechanism due to debondment propagation at the interface. Debondment propagation at the interface is one of the main mechanisms for the failure of coating–substrate system. It is well known that strain energy release rate G is a measure of the driving force for debondment propagation. When G attains its critical value G_{cr} , the debondment propagates. In case of debonding in a homogeneous solid body, G_{cr} is a material constant, while for interface crack it is dependent on some interface parameters such as phase angle ψ . By incorporating Equation (27), Hutchinson's equation for elastic energy release rate G can be modified to redefine the debondment propagation problem in terms of concentration of diffusing substance k , such that,

$$G' = \frac{\partial G}{\partial t} = \frac{6(1 - \nu^2)}{Eh^3} M_c^2 \left[1 + \left(k_1 \sqrt{(\Omega - 1)}\right)^2\right] \quad (28)$$

where $G' = \frac{\partial G}{\partial t}$ is the change in strain energy release rate with time which depends on the change in diffusion-induced stress with time, $\Omega = \frac{\sigma'_{dc}}{\sigma_{cr}}$, $M_c = \frac{c'_{kc} h}{2}$ is the applied moment of coating having thickness h ; $k_1 = 0.5 \sqrt{\frac{(1+\nu)^2}{(1+\nu)+(1-\nu)}}$ is the constant which depends upon Poisson's ratio of the coating.

G' in Equation (28) can be associated with mode-mix function j and Γ_{IC} when condition $\Omega \geq \Omega_{cr}$ is met. Where Γ_{IC} is the mode I toughness.[58] Associating G' with j makes the strain energy release rate G' mode dependent, such that,

$$G' = \Gamma_{IC} j \quad (29)$$

Mode-dependent strain energy release rate G' due to debonding can be adjusted using a dimensionless mode-mix function j . Debondment propagation depends on mode-adjusted debonding driving force F ,[62] such that,

$$F = \frac{G'}{j} \quad (30)$$

The incipient requirement for debondment to propagate follows the condition $j \rightarrow 1$. Upon substituting $j \rightarrow 1$ in Equation (29), the incipient requirement becomes $G' \approx \Gamma_{IC}$.

The value for incipient propagation of debondment is the critical value of G' i.e. G_{cr} . The value of ‘intrinsic-toughness’ Γ_{IC} is always equal to G_{cr} at the tip i.e. $G_{cr} \approx \Gamma_{IC}$. [62] Γ_{IC} is found by utilising Equation (29) specific to the condition $j \rightarrow 1$ as,

$$\Gamma_{IC} = [G' \rightarrow 0] \quad \text{if } j \rightarrow 1 \quad (31)$$

where $G' \rightarrow 0$ means that G' exhibit an extremely small value, approaching to zero but is not exactly zero. Similarly, $j \rightarrow 1$ means that the value of j approaches to 1 but is not exactly 1.

The mode-mix function j is given as:

$$j = \sec^2 \left[\left(1 - \frac{\Gamma_{IC}}{E_1 \lambda} \right) \psi \right] \quad (32a)$$

$$\psi = \cot \frac{\cos \omega + (0.2486(1 + \nu)\mathbb{H})\sin \omega}{(0.2486(1 + \nu)\mathbb{H})\cos \omega - \sin \omega} \quad (32b)$$

where λ in Equation (32a) represents the interface roughness; parameter ω in Equation (32b) is dependent upon Dundur’s elastic mismatch parameter χ . [59] where $\chi = (\bar{E}_1 - \bar{E}_2)/(\bar{E}_1 + \bar{E}_2)$. [63] The ‘intrinsic toughness’ Γ_{IC} which is found in Equation (31) is utilised in the term $1 - \frac{\Gamma_{IC}}{E_1 \lambda}$ in Equation (32a).

The mode adjustment term (phase angle), ψ in Equation (32b) defines the mode (mode I or mode II) of debondment propagation. Interface is tougher in mode I compared to mode II. The mode adjustment term ψ is adjustable by using deflection index parameter \mathbb{H} where \mathbb{H} depends on \cap and is given as [62]:

$$\mathbb{H} = k_2 \sqrt{(\cap - 1)} \quad (33)$$

where $k_2 = \sqrt{[0.2(1 + \nu) + (1 - \nu^2)]^{-1}}$ is the constant which depends upon the value of Poisson’s ratio.

The partial differential equation (PDE) for debonding driving force F can be determined from the solution of Equation (28), (30), (32a) and (32b) as:

$$F(\lambda, h) = \frac{G'(h)}{j(\lambda)} = \frac{k_3 c_{k_c}^2 + k_3 c_{k_c}^2 k_1^2 (\cap(h) - 1)}{4h \left[\sec^2 \left[\left(1 - B \right) \cot \frac{\cos \omega + k_4 \sqrt{(\cap(h) - 1)} \sin \omega}{k_4 \sqrt{(\cap(h) - 1)} \cos \omega - \sin \omega} \right] \right]} \quad (34)$$

where $k_3 = \frac{6(1 - \nu^2)}{E_c}$; $k_4 = 0.25(1 + \nu)k_2$ and $B = \frac{\Gamma_{IC}}{E_c \lambda}$ as $\lambda = \frac{R_a^2}{L_a}$ (R_a = Average roughness amplitude; L_a = Average roughness wavelength).

It is worth noting that equation depends on the concentration of diffusing substance $c_{k_c}^2$ which if becomes zero makes $F(\lambda, h) = 0$. It is clear that the above equation agrees with Hutchinson et al. [58] for the same crack propagation problem when $\cap(h)$ is replaced with $\frac{\sigma}{\sigma_{cr}}$ and $\frac{c_{k_c} h}{2}$ is replaced with M_c .

$F(\lambda, h)$ in Equation (34) is a function of two parameters i.e. interface roughness λ and coating thickness h . It is important to note that interface roughness λ only effects the magnitude of debonding driving force F with no influence on time discretisation, while coating thickness h effects the time discretisation of debonding driving force F . The ‘variation in magnitude’ of debonding driving force F is performed by utilising mode-mix function $j(\lambda)$. Where $j(\lambda)$ is a function of only one parameter i.e. interface roughness λ . Where $j(\lambda)$ adjusts the mode of debondment propagation (mode I or mode II). However, ‘time dependent’ variation of debonding driving force F is performed by

varying $\cap(h)$ which effects $G'(h)$. Where $\cap(h)$ is a function of only one parameter i.e. coating thickness h .

Equation (34) can be utilised to find the critical values of debonding driving force F_{cr} , interface roughness λ_{cr} and coating thickness h_{cr} for the two set-ups of experiment as follows.

Set-up 1: Constant h with variable λ – finding critical/threshold value

$\lambda = \lambda_{cr}$ is found against the condition when $F(\lambda)$ approaches to $G'(h)$ i.e. $F(\lambda) \rightarrow G'(h)$ in Equation (34). This is only possible when $j(\lambda) \rightarrow 1$. $G'(h)$ is calculated using Equation (28). Therefore, for condition $\lambda = \lambda_{cr}$, the value of adjusted magnitude of $F(\lambda)$ by adjusting $j(\lambda) \rightarrow 1$ (in $F(\lambda) = G'(h)/j(\lambda)$) always approaches to $G'(h)$. This is actually the critical value of debonding driving force which is a function of λ_{cr} and is represented as $F_{cr}(\lambda_{cr}) = [F(\lambda) \rightarrow G'(h)]$. The generalised equation for finding $F_{cr}(\lambda_{cr})$ is given in Equation (35a) which is derived from Equation (34).

If variation of λ becomes greater than λ_{cr} , then $j(\lambda)$ starts to increase and magnitude of $F(\lambda)$ starts to decrease which becomes much smaller compared to $G'(h)$ therefore, making interface more and more tougher.

$$F_{cr}(\lambda_{cr}) = \frac{k_3 c_{k_c}^2 + k_3 c_{k_c}^2 k_1^2 (\cap(h) - 1)}{4h} \quad (35a)$$

If variation in λ becomes less than λ_{cr} , then $j(\lambda)$ starts to decrease and magnitude of $F(\lambda)$ starts to increase resulting in coating debondment.

Set-up 2: Constant λ with variable h – finding critical/threshold value

$h = h_{cr}$ is found against the condition when $\cap(h) = 1$, which upon substitution in Equation (34) gives Equation (35b). The expression on right-hand side of Equation (35b) returns the critical value of F . This critical value of debonding driving force is a function of h_{cr} and is represented as $F_{cr}(h_{cr})$. Variation in h effects the variation of F with respect to time.

If variation of h becomes less than h_{cr} , then $\cap(h)$ starts to increase, causing time-dependent debonding driving force $F(h)$ to increase which results in the coating debondment.

$$F_{cr}(h_{cr}) = \frac{k_3 c_{k_c}^2}{4h_{cr} [\sec^2 [(1 - B) \cot \frac{\cos \omega}{\sin \omega}]]} \quad (35b)$$

The reasons that why thicker coatings ($h \gg h_{cr}$) possess lower debonding driving force F are as follows: (i) $\cap(h)$ is a direct function of bending curvature of coating $\frac{1}{\zeta}$ which inversely relates with the thickness of coating h as clear from Equation (23) and (ii) critical stress of the coating σ_{cr} increases with an increase in h which again reduces $\cap(h)$ and ultimately results in lower $F(h)$.

5. Mathematical model solution and implementation

The initial and boundary conditions for the stressed cantilever are expressed as follows:

$$c'_{k_c}(x) = c'_{k_s}(x) = 0; \quad \lambda = h = 0 \quad \text{and} \quad D_{k_c} = D_{k_s} = 0 \quad \text{at time } t = 0 \quad (36)$$

$$\frac{\partial c'_{k_s}}{\partial x} \Big|_{x=s} = 0; \quad c'_{k_c}(h) = c_{k_o} \quad \text{at time } t > 0 \quad (37)$$

For numerical simulation work, all the parameters and variables, which are used in the equations, should be converted into dimensionless forms as:

$$\tilde{D}_k = D_{k_c}/D_{k_s} \tag{38a}$$

$$\tilde{x} = \frac{x}{b} = \frac{x}{h+s} \tag{38b}$$

$$\tilde{C}'_{k_c} = c'_{k_c}/c_{k_o}; \quad \tilde{C}'_{k_s} = c'_{k_s}/c_{k_o} \tag{38c}$$

$$\tilde{t} = D_{k_c}t/b^2 \tag{38d}$$

$$\tilde{A} = \left(\frac{E_c \overline{V_{P_{k_c}}}}{RT} \right) c_{k_o} = \left(\frac{E_s \overline{V_{P_{k_c}}}}{RT} \right) c_{k_o} \tag{38e}$$

$$\frac{1}{\zeta} = \frac{b}{\zeta \overline{V_{P_k}} c_{k_o}} = \frac{4(1+1/\eta)^3 (1+(\Lambda^{-1}/\eta)) \left(\Lambda^{-1} \int_0^{\frac{1/\eta}{1/\eta+1}} \tilde{c}'_{k_s} x' dx' + \int_0^{\frac{1}{1/\eta+1}} \tilde{c}'_{k_c} x' dx' \right)}{\left(\Lambda^{-1} \left(\frac{1}{\eta} \right)^2 - 1 \right)^2 + 4\Lambda^{-1} \left(\frac{1}{\eta} \right) \left(\frac{1}{\eta} + 1 \right)^2} \tag{38f}$$

$$- \frac{2 \left(1 - \Lambda^{-1} \left(\frac{1}{\eta} \right)^2 \right) \left(1 + \frac{1}{\eta} \right)^2 \left(\Lambda^{-1} \int_0^{\frac{1/\eta}{1/\eta+1}} \tilde{c}'_{k_s} x' dx' + \int_0^{\frac{1}{1/\eta+1}} \tilde{c}'_{k_c} x' dx' \right)}{\left(\Lambda^{-1} \left(\frac{1}{\eta} \right)^2 - 1 \right)^2 + 4\Lambda^{-1} \left(\frac{1}{\eta} \right) \left(\frac{1}{\eta} + 1 \right)^2}$$

$$\tilde{k}_3 = \left(\frac{6(1-\nu^2)}{\Lambda^{-1}} \right) = \left(\frac{6(1-\nu^2)}{E_c} \right) E_s \tag{38g}$$

$$\tilde{\lambda} = R_a/L_a \tag{38h}$$

$$\tilde{B} = \frac{\tilde{G}_{cr}}{\Lambda^{-1} \tilde{\lambda}} = \frac{\tilde{G}_{cr} E_s L}{R E_c} \tag{38i}$$

$$\tilde{F}(\tilde{\lambda}, h) = \frac{\tilde{G}'(h)}{j(\tilde{\lambda})} = \frac{\tilde{k}_3 \tilde{c}'_{k_c} 2 + \tilde{k}_3 \tilde{c}'_{k_c}{}^2 k_1^2 (\cap(h) - 1)}{4/\eta \left[\sec^2 \left[\left(1 - \tilde{B} \right) \cot \frac{\cos \omega + k_4 \sqrt{(\cap(h)-1) \sin \omega}}{k_4 \sqrt{(\cap(h)-1) \cos \omega - \sin \omega}} \right] \right]} \tag{38j}$$

$$\tilde{F}_{cr}(\tilde{\lambda}_{cr}) = \frac{\tilde{k}_3 \tilde{c}'_{k_c}{}^2 + \tilde{k}_3 \tilde{c}'_{k_c}{}^2 k_1^2 (\cap(h) - 1)}{4/\eta} \tag{38k}$$

$$\tilde{F}_{cr}(h_{cr}) = \frac{\tilde{k}_3 \tilde{c}'_{k_c}{}^2}{4/\eta_{cr} \left[\sec^2 \left[\left(1 - \tilde{B} \right) \cot \frac{\cos \omega}{-\sin \omega} \right] \right]} \tag{38l}$$

where $\Lambda^{-1} = E_c/E_s$; $1/\eta = h/s$; $1/\eta_{cr} = h_{cr}/s = (h/s)_{cr}$ and it is assumed that $\overline{V_{P_k}} = \overline{V_{P_{k_c}}} = \overline{V_{P_{k_s}}}$.

In this research, the newly developed algorithm follows a ‘two set-up approach’. The two set-ups can be generalised by utilising a PDE in Equation (38j) as:

$$\tilde{F}(\tilde{\lambda}) = \tilde{F}(N) \quad (\text{Set-up 1}) \quad (39a)$$

$$\frac{\partial \tilde{F}}{\partial t}(h) = \tilde{F}^i(n) \quad (\text{Set-up 2}) \quad (39b)$$

Set-up 1 consists of a simple iterative method to update the value of interface roughness $\tilde{\lambda}$ which is represented by variable N in Equation (39a). This set-up is highlighted as an olive green box in Figure 5. The iteration of $\tilde{\lambda}$ is used only to adjust the ‘magnitude’ of debonding driving force \tilde{F} but has no influence on the time

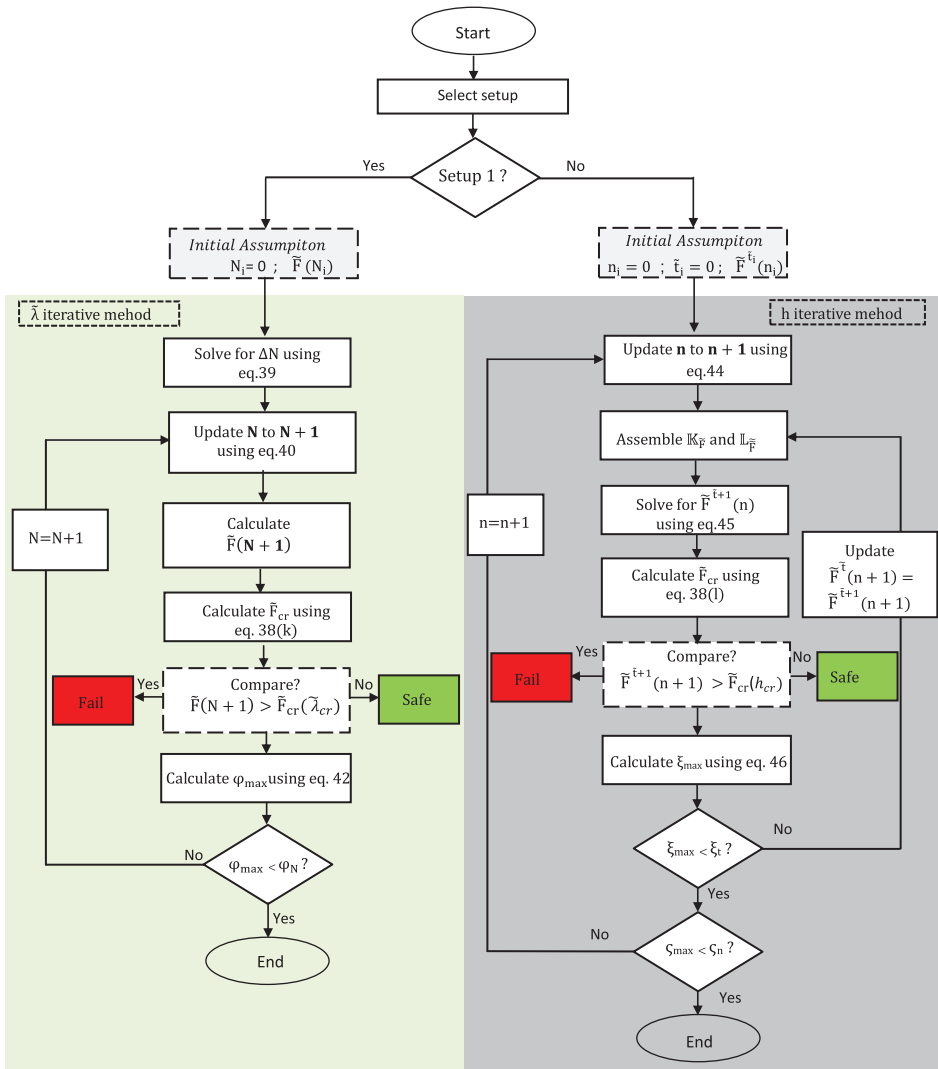


Figure 5. Algorithm for a two set-up approach used for estimating the debonding driving force as a function of interface roughness (using set-up 1) and coating thickness (using set-up 2).

discretisation of \tilde{F} . The only parameter which influences the ‘time discretisation’ of \tilde{F} is the coating thickness h which is generalised in Equation (39b) under set-up 2. The iterations of h are represented by n and the time states are represented by superscript \tilde{t} . Newton–Rhapson method [64] is utilised to solve the time-varying PDE $\frac{\partial F}{\partial t}$. The governing PDE $\frac{\partial F}{\partial t}$ for normalised debonding driving force \tilde{F} in the domain is discretised in time and space and cast into the matrix form using Newton–Rhapson method. This set-up is highlighted as grey box in Figure 5.

The two set-up algorithm follows the following steps.

- (i) The algorithm starts with the selection of set-up. Set-up 1 is used to analyse the effect of $\tilde{\lambda}$ on \tilde{F} while set-up 2 is used to analyse the effect of h on \tilde{F} .
- (ii) If set-up 1 is selected than the algorithm enters into set-up 1 ($\tilde{\lambda}$ iteration). The initial assumed value for variable N is set as $N_i = 0$ using the boundary conditions in stressed cantilever as mentioned in Equation (36).
- (iii) Next, the algorithm initialises the iterative process for a parameter $\tilde{\lambda}$. The algorithm computes ΔN as:

$$\Delta N = N - N_i, \text{ where } N_i = 0 \quad (40)$$

- (iv) This initially computed ΔN is used every time to update N to the next level, $N + 1$ using,

$$N + 1 = N + \Delta N \quad (41)$$

- (v) For an updated $N + 1$, the algorithm calculates the normalised debonding driving force $\tilde{F}(N + 1)$ and then compares this value with the critical value of normalised debonding driving force $\tilde{F}_{cr}(\tilde{\lambda}_{cr})$. Where $\tilde{F}_{cr}(\tilde{\lambda}_{cr})$ is calculated using Equation (38k). On comparison, if $\tilde{F}(N + 1) > \tilde{F}_{cr}(\tilde{\lambda}_{cr})$, then the algorithm returns the ‘Safe condition’ however, if $\tilde{F}(N + 1) < \tilde{F}_{cr}(\tilde{\lambda}_{cr})$, then the algorithm returns the ‘Fail condition’.
- (vi) The interface roughness convergence criterion for variable N is calculated as:

$$\varphi_N = 100 \left[\frac{g^{N+1} - g^N}{g^N} \right] \quad (42)$$

where g is a generic term representing $\tilde{\lambda}$. For the condition $\varphi_{\max} > \varphi_N$, the value of $\tilde{\lambda}$ is updated, and control is returned to step (iv). For the condition $\varphi_{\max} < \varphi_N$, the algorithm for set-up 1 ends.

- (vii) If set-up 2 is selected than the algorithm enters into set-up 2 (h iteration). The algorithm initialises the iterative process for a parameter h . The algorithm computes Δn as:

$$\Delta n = n - n_i \quad \text{where } n_i = 0 \quad (43)$$

- (viii) This initially computed Δn is used every time to update n to the next level $n + 1$ using,

$$n + 1 = n + \Delta n \quad (44)$$

- (ix) The initial time value ($\tilde{t}_1 = 0$) for $\tilde{F}^{\tilde{t}}(n)$ is assumed as $\tilde{F}^o(n)$ using the boundary conditions in stressed cantilever as mentioned in Equation (36).
 (x) The governing equation and boundary conditions for \tilde{F} are time discretised and cast into the matrix form as:

$$\mathbb{K}_{\tilde{F}} \tilde{F}^{\tilde{t}+1}(n) = \mathbb{L}_{\tilde{F}}, \quad (45)$$

where $\mathbb{K}_{\tilde{F}}$ is the coefficient matrix and is a function of $\tilde{F}^{\tilde{t}+1}$ at time state $\tilde{t}+1$ and \mathbb{L} is the load vector and is a function of $\tilde{F}^{\tilde{t}}(n)$ at time state \tilde{t} . Based on matrices $\mathbb{K}_{\tilde{F}}$ and $\mathbb{L}_{\tilde{F}}$, the value of $\tilde{F}^{\tilde{t}+1}$ is computed.

- (xi) For an updated $\tilde{F}^{\tilde{t}+1}$, the algorithm compares this value with the critical value of normalised debonding driving force $\tilde{F}_{\text{cr}}(h_{\text{cr}})$. Where $\tilde{F}_{\text{cr}}(h_{\text{cr}})$ is calculated using Equation (381). On comparison if $\tilde{F}^{\tilde{t}+1}(n) > \tilde{F}_{\text{cr}}(h_{\text{cr}})$, then the algorithm returns the ‘Safe condition’ however, if $\tilde{F}^{\tilde{t}+1} < \tilde{F}_{\text{cr}}(h_{\text{cr}})$, then the algorithm returns the ‘Fail condition’.
 (xii) The time convergence criterion is calculated as:

$$\xi_{\tilde{t}} = 100 \left[\frac{f^{\tilde{t}+1} - f^{\tilde{t}}}{f^{\tilde{t}}} \right] \quad (46)$$

where f is a generic term representing \tilde{t} . The value of f for at each time state in the domain, except on the boundary conditions, was calculated and the maximum value of ξ_{max} , was determined. The value of ξ_{max} is compared with a convergence criterion ξ_n . For the condition $\xi_{\text{max}} > \xi_n$, the value of \tilde{t} is updated, and control returned to step (x). For the condition $\xi_{\text{max}} < \xi_n$, the algorithm moves to next step.

- (xiii) The thickness convergence criterion for variable n is calculated as:

$$\varsigma_n = 100 \left[\frac{m^{n+1} - m^n}{m^n} \right] \quad (47)$$

where m is a generic term representing h . For the condition $\varsigma_{\text{max}} > \varsigma_n$, the value of h is updated, and control returned to step (viii). For the condition $\varsigma_{\text{max}} < \varsigma_n$, the algorithm for set-up 2 ends.

6. Simulation results and discussion

6.1. Simulation results of set-up 1

For the case of relative coating thickness h/s being fixed, the effects of normalised interface roughness, $\tilde{\lambda}$, on normalised debonding driving force \tilde{F} are analysed using

set-up 1 algorithm. These results are shown in Figure 6, where $\tilde{A} = 0.5$, $\Lambda^{-1} = E_c/E_s = 1$, $\tilde{k}_3 = 5$, $\tilde{D}_k = D_{k_c}/D_{k_s} = 10$, $1/\eta = h/s = 0.1$ and $T/T_o = \text{constant}$, where T_o is absolute temperature. From Figure 6, it is clear that the debonding driving force \tilde{F} decreases with an increase in interface roughness $\tilde{\lambda}$ and becomes stable after certain value of $\tilde{\lambda}$. The debonding driving force \tilde{F} as a function of interface roughness $\tilde{\lambda}$ is time independent. Similar curves of \tilde{F} corresponding to time steps $D_{k_c}t/b^2 = 0.05$ to 0.25 are observed which are shown in Figure 6.

Figure 6 shows the coating fail, critical and safe conditions in terms of debonding driving force \tilde{F} and interface roughness $\tilde{\lambda}$. When the interface roughness $\tilde{\lambda}$ is greater than critical $\tilde{\lambda}_{cr}$ and the corresponding debonding driving force \tilde{F} is less than critical \tilde{F}_{cr} , then the coating is considered to be safe and are represented as: $\tilde{\lambda}_s, \tilde{F}_s$. Conversely, if $\tilde{\lambda}$ is less than critical $\tilde{\lambda}_{cr}$ and corresponding \tilde{F} is greater than critical \tilde{F}_{cr} , then the coating is considered to be fail and are represented as: $\tilde{\lambda}_f, \tilde{F}_f$. Where, $\tilde{\lambda}_{cr} = 0.2$ and $\tilde{F}_{cr} = 0.3$ are said to be critical points for coating failure. This indicates that increasing the interface roughness is better in order to avoid coating debondment from substrate. However, this is subject to condition that the coating and substrate properties like thickness, Young's modulus and diffusivity should remain constant with an increase in interface roughness.

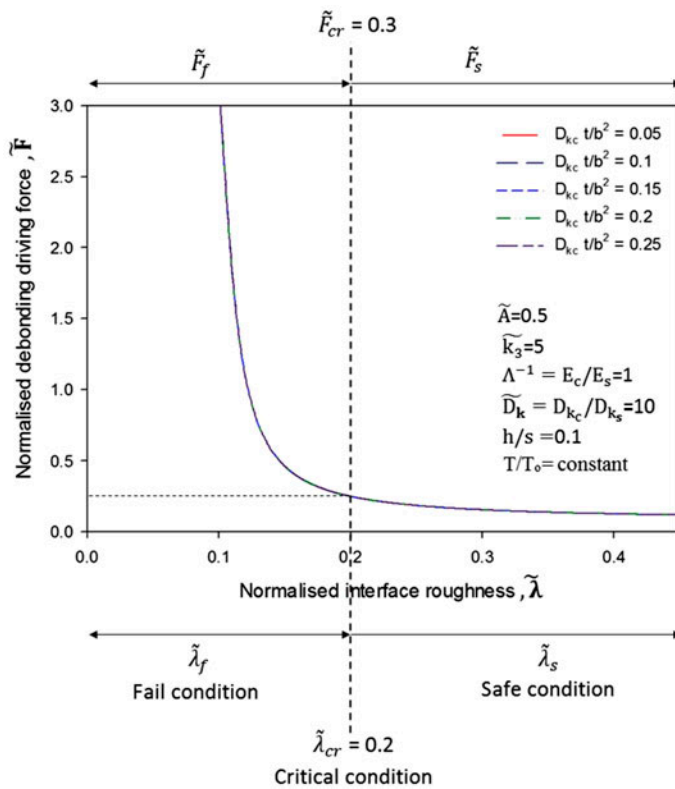


Figure 6. Simulation graph using set-up 1: Debonding driving force \tilde{F} as a function of normalised interface roughness $\tilde{\lambda}$ keeping constant value of relative coating thickness h/s . Simulation graph showing time independent behaviour of \tilde{F} for various values of time $D_{k_c}t/b^2$. Simulation graph also defines safe, critical and fail conditions for coating performance.

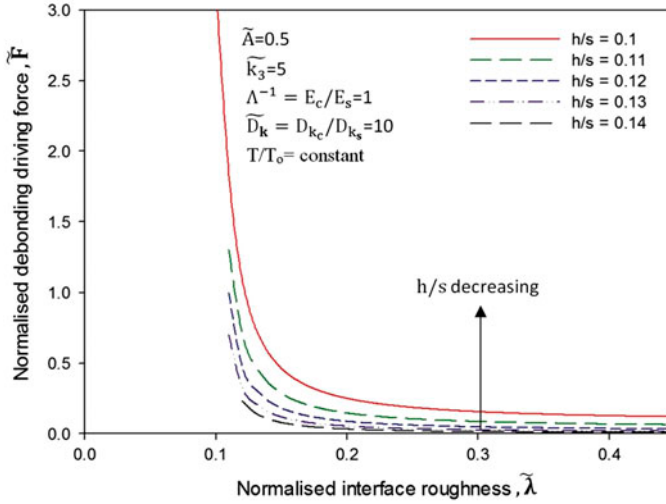


Figure 7. Evolution of normalised debonding driving force \tilde{F} corresponding to various values of relative coating thickness h/s and normalised interface roughness $\tilde{\lambda}$.

Figure 7 shows the evolution of debonding driving force \tilde{F} corresponding to various values of relative coating thickness h/s and normalised interface roughness $\tilde{\lambda}$. Where $\tilde{A} = 0.5$, $\Lambda^{-1} = E_c/E_s = 1$, $\tilde{k}_3 = 5$, $\tilde{D}_k = D_{k_c}/D_{k_s} = 10$ and $T/T_o = \text{constant}$. Separate numerical simulation was conducted for this purpose apart from the set-up 1 algorithm in Figure 5. It is worth noting that the effect of normalised coating thickness h/s on debonding driving force \tilde{F} is dominant at lower interface roughness, when interface roughness $\tilde{\lambda}$ is less than 0.2. However, the debonding driving force \tilde{F} becomes stable and becomes independent of the value of normalised coating thickness h/s at higher interface roughness $\tilde{\lambda}$, greater than 0.2. This means that at higher interface roughness, the coating-substrate system becomes independent of the value of coating thickness. This is the reason that for some coating-substrate systems, the debonding driving force is independent of the coating thickness. It can also be concluded from Figure 7 that at lower interface roughness $\tilde{\lambda} < 0.2$, where it is expected that debonding driving force will be high, the debonding driving force can be minimised by increasing the coating thickness. However, this is subject to condition that Young's modulus and diffusivity of coating should not change with an increase in interface roughness and coating thickness.

6.2. Simulation results of set-up 2

For the case of interface roughness $\tilde{\lambda}$ and substrate thickness s being fixed, the effects of relative coating thickness, h/s , on normalised debonding driving force \tilde{F} are analysed using set-up 2 algorithm. These results are shown in Figure 8, where $\tilde{A} = 0.5$, $\Lambda^{-1} = E_c/E_s = 1$, $\tilde{k}_3 = 5$, $\tilde{D}_k = D_{k_c}/D_{k_s} = 10$, $\tilde{B} = \frac{\Gamma_{1c}}{E_c \lambda} = 0.5$ and $T/T_o = \text{constant}$, where T_o is absolute temperature. It is assumed that the diffusivity D_{k_c} of the coating is 10 times more compared to the diffusivity D_{k_s} of the substrate and therefore, leads to $\tilde{D}_k = 10$. From Figure 8, it is observed that the debonding driving force \tilde{F} decreases

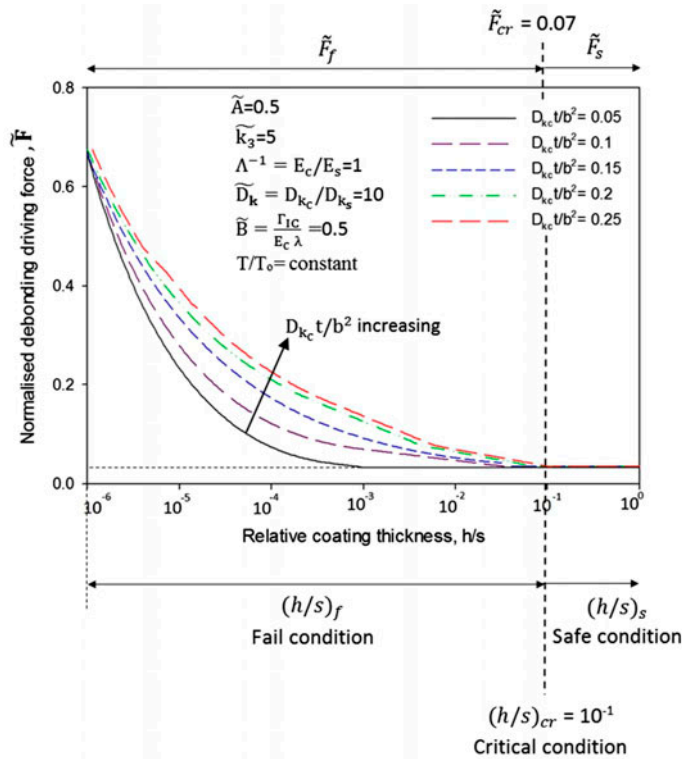


Figure 8. Simulation graph using set-up 2: Normalised debonding driving force \tilde{F} as a function of relative coating thickness h/s keeping constant value of normalised interfacial roughness $\tilde{\lambda}$. Simulation graph showing time discretisation of \tilde{F} for various values of h/s . Simulation graph also defines safe, critical and fail conditions for coating performance.

with increasing the relative coating thickness, h/s . The relative coating thickness increases with an increase in h because s is constant and is assumed to be large. This indicates that increasing the thickness of coating h is better in order to avoid coating debondment from substrate. However, this is subject to condition that the diffusivity D_{k_c} should not increase and Young's modulus E_c should not decrease with an increase in the thickness h . If diffusivity D_{k_c} of the coating increases with an increase in thickness h , then this means that coating is becoming more permeable to diffusing component and therefore, leads to coating failure. If Young's modulus E_c of the coating decreases with an increase in thickness h than this means that the flexibility of coating is increasing which results in higher debonding driving force and in turn results in coating failure.

Comparatively, for a less relative coating thickness, i.e. $h/s < 10^{-1}$, debonding driving force \tilde{F} will increase with increasing the time at a given h/s . However, a time-independent debonding driving force \tilde{F} is observed when the thickness h of coating is either very small ($h/s < 10^{-6}$) or comparable ($h/s > 10^{-1}$) to the thickness s of the substrate. Figure 8 indicates the coating fail, critical and safe conditions in terms of debonding driving force \tilde{F} and relative coating thickness h/s . When the relative coating thickness h/s is greater than 10^{-1} and the corresponding debonding driving force \tilde{F} is less than 0.07,

then the coating is considered to be safe and is represented as: $(h/s)_s, \tilde{F}_s$. Conversely, if h/s is less than 10^{-1} and corresponding \tilde{F} is greater than 0.07, then the coating is considered to be fail and are represented as: $(h/s)_f, \tilde{F}_f$. Where $(h/s)_{cr} = 10^{-1}$ and $\tilde{F}_{cr} = 0.07$ are said to be critical points for coating failure.

It is important to analyse the effects of diffusivity ratio D_{k_c}/D_{k_s} on debonding driving force \tilde{F} , therefore, a separate numerical simulation was conducted for this purpose apart from the set-up 2 algorithm in Figure 5. For a given diffusivity of substrate D_{k_s} , the effects of the diffusivity ratio, D_{k_c}/D_{k_s} , on the debonding driving force \tilde{F} are shown in Figure 9, where $\tilde{A} = 0.5$, $\tilde{k}_3 = 5$, $h/s = 10^0 = 1$, $\Lambda^{-1} = E_c/E_s = 1$, $\tilde{B} = \frac{\Gamma_{lc}}{E_c \lambda} = 0.5$ and $T/T_o = \text{constant}$. From Figure 9, it is evident that the trends for debonding driving force \tilde{F} are identical for various ratios of diffusivity corresponding to the very short diffusing time i.e. $D_{k_c}t/b^2 = 0.02$. After then, the debonding driving force \tilde{F} reaches a maximum and then decreases gradually with increasing the time, especially for the small ratio of diffusivity, D_{k_c}/D_{k_s} . However, the debonding driving force \tilde{F} remains constant for higher ratio of diffusivity. This indicates that in order to avoid high and stable debonding driving force \tilde{F} , the diffusivity of coating D_{k_c} should be kept small by the manufacturers guaranteeing least permeability to diffusing substance k .

Similar analysis, like that of D_{k_c}/D_{k_s} , was also performed for E_c/E_s . Figure 10 shows the evolution of debonding driving force \tilde{F} corresponding to various Young's modulus ratios, E_c/E_s where $\tilde{A} = 0.5$, $\tilde{k}_3 = 5$, $h/s = 10^0 = 1$, $\tilde{D}_k = D_{k_c}/D_{k_s} = 10$, $\tilde{B} = \frac{\Gamma_{lc}}{E_c \lambda} = 0.5$ and $T/T_o = \text{constant}$. As shown in Figure 10, the debonding driving force \tilde{F} increases sharply to a maximum and then becomes stable with an increase in time. It is worth noting that the debonding driving force \tilde{F} increases with decreasing the ratio of Young's modulus, E_c/E_s . This indicates that for a given thickness h and concentration of diffusing substance, decreasing the flexibility of coating by increasing the Young's modulus E_c can reduce the debonding driving force \tilde{F} . This increase in Young's modulus E_c of coating will improve the adhesion of coating with substrate.

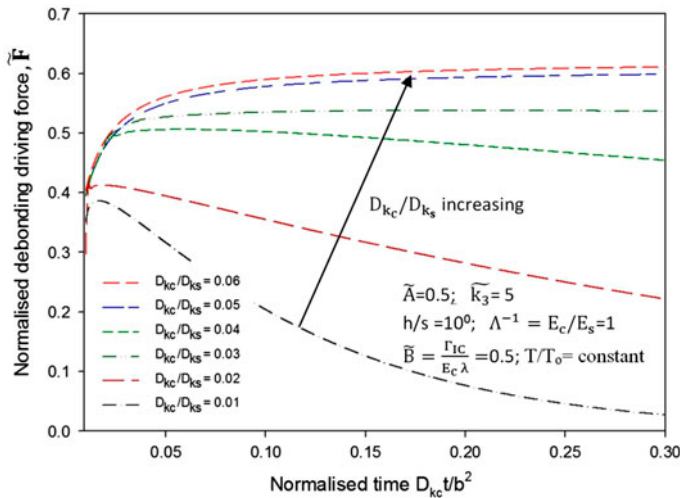


Figure 9. Effects of diffusivity ratio D_{k_c}/D_{k_s} of coating and substrate on normalised debonding driving force \tilde{F} .

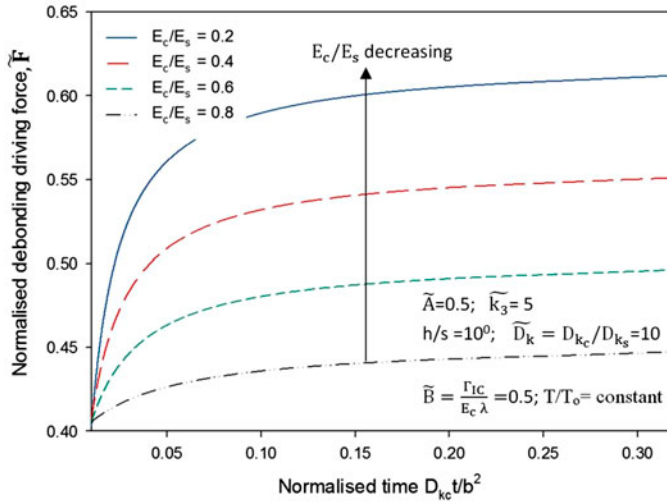


Figure 10. Effects of Young’s modulus ratio E_c/E_s of coating and substrate on normalised debonding driving force \bar{F} .

7. Reliability assessment model (application of failure prediction model)

Interface roughness and coating thickness are the two most important parameters that contribute towards the failure of coating–substrate system. Therefore, during the design process, the manufacturers must be aware of the reliability of coating–substrate system, which is being manufactured. The reliability assessment [65] for coating–substrate system is performed using a probabilistic approach. The assessment is based on failure prediction model (in Section 4). The reliability assessment model can further be utilised in prognostics which is defined as the ability to predict accurately and precisely the remaining useful life of a failing component or system.[66] In this research, the failing system is coating–substrate system.

7.1. Debondment initiation

The debonding driving force equal to its critical value is the incipient requirement for the initiation of coating debondment. The PDE ($f(x)$) for the debonding driving force (in Equation (34)) is a probability density function [67,68] over the range of X_0 to X_{cr} . The limits X_0 and X_{cr} represent the initial and critical values, respectively, for variables λ and h . The cumulative density function $R_{init}(X)$ is,

$$R_{init}(X) = \int_{X_0}^{X_{cr}} f(x) dx \tag{48}$$

where $R_{init}(X)$ represents the value of debonding driving force at which the debondment initiates. This is actually the point of failure for coating–substrate system.

7.2. Instantaneous failure probability

The instantaneous failure probability $P(X)$ of coating–substrate system is the ratio of probability of failure due to debonding driving force to the probability of use without failure $N(X) = 1 - R_{init}(X)$, so

$$f(x) = \frac{d}{dX} R_{\text{init}}(X) \quad (49)$$

$$P(X) = \frac{f(x)}{1 - R_{\text{init}}(X)} = \frac{f(X)}{N(X)} \quad (50)$$

where R_{init} is the commutative density function and is found using Equation (48).

8. Conclusions

A failure prediction and reliability assessment model for coating–substrate system has been developed based on a multidisciplinary approach. Coating–substrate adhesion depends on the debonding driving force. Higher debonding driving force accounts for low interface adhesion and vice versa. A mathematical equation for debonding driving force is developed incorporating the concepts of material science and solid mechanics. The equation is further modified to find the critical value of debonding driving force. This critical value defines the point of failure and is utilised to evaluate the performance of coating–substrate system i.e. safe, critical and fail. The model is also used to assess the reliability of coating–substrate system which can be used by the manufacturers during the design process. Interface roughness and coating thickness are two most important parameters which influence the performance of coating–substrate system. The debonding driving force decreases with an increase in the interface roughness and coating thickness. However, this is subject to condition that the material properties of coating such as, diffusivity D_{k_c} should not increase and Young’s modulus E_c should not decrease with an increase in the interface roughness and coating thickness. For example, if diffusivity D_{k_c} of the coating increases with an increase in coating thickness, then this means that coating is becoming more permeable to diffusing component and therefore, leads to coating failure. Likewise, if Young’s modulus E_c of the coating decreases with an increase in coating thickness then this means that the susceptibility to failure of coating is increasing which results in higher debonding driving force and in turn results in coating failure. Therefore, for best performance of coating–substrate system, it is important to keep diffusivity low and Young’s modulus high while increasing interface roughness and coating thickness.

The model is developed based on the observation recorded from experimentation. The experiment involved the sample preparation according to the ‘two set-up approach’ i.e. (i) set-up 1: constant coating thickness with variable interface roughness and (ii) set-up 2: constant interface roughness with variable coating thickness. The experiments comprised of Vickers indentation test and ASTM-B117 test. These experiments were performed to understand the behaviour of debonding driving force with the variation in interface roughness and coating thickness under two set-ups, respectively.

Acknowledgements

This research is joint funded by Defence Science and Technology Laboratory (DSTL), Ministry of Defence (MoD) and Bournemouth University UK. The authors acknowledge their support and contributions.

Funding

This research is joint funded by Defence Science and Technology Laboratory (DSTL), Ministry of Defence (MoD) and Bournemouth University UK.

References

- [1] Koleske JV. Paint and coating testing manual: fifteenth edition of the Gardner-Sward handbook. Vol. 17. ASTM International; 1995. Available from: http://www.astm.org/DIGITAL_LIBRARY/MNL/SOURCE_PAGES/MNL17-2ND_foreword.pdf
- [2] Balslev I. Influence of uniaxial stress on the indirect absorption edge in silicon and germanium. *Phys. Rev.* 1966;143:636–647.
- [3] Begley MR, Utz M. Multiscale modeling of adsorbed molecules on freestanding microfabricated structures. *J. Appl. Mech.* 2008;75:021008.
- [4] Mahmoodi SN, Afshari M, Jalili N. Nonlinear vibrations of piezoelectric microcantilevers for biologically-induced surface stress sensing. *Commun. Nonlinear Sci. Numer. Simul.* 2008;13:1964–1977.
- [5] Tsui Y, Doyle C, Clyne T. Plasma sprayed hydroxyapatite coatings on titanium substrates. Part 1: mechanical properties and residual stress levels. *Biomaterials.* 1998;19:2015–2029.
- [6] Hainsworth S, McGurk M, Page T. The effect of coating cracking on the indentation response of thin hard-coated systems. *Surf. Coat. Technol.* 1998;102:97–107.
- [7] Clyne T, Gill S. Residual stresses in thermal spray coatings and their effect on interfacial adhesion: a review of recent work. *J. Therm. Spray Technol.* 1996;5:401–418.
- [8] Clyne T. Residual stresses in surface coatings and their effects on interfacial debonding. *Key Eng. Mater.* 1995;116:307–330.
- [9] Tsui Y, Clyne T. An analytical model for predicting residual stresses in progressively deposited coatings. Part 1: planar geometry. *Thin Solid Films.* 1997;306:23–33.
- [10] Howard S, Tsui Y, Clyne T. The effect of residual stresses on the debonding of coatings – I. A model for delamination at a bimaterial interface. *Acta Metall. Mater.* 1994;42:2823–2836.
- [11] Podstrigach YS, Shevchuk P. Effect of surface layers on diffusion processes and the resulting stress state in solids. *Soviet Mater. Sci.* 1968;3:420–426.
- [12] Ida Y. Thermodynamic theory of nonhydrostatically stressed solid involving finite strain. *J. Geophys. Res.* 1969;74:3208–3218.
- [13] Larché F, Cahn J. A linear theory of thermochemical equilibrium of solids under stress. *Acta Metall.* 1973;21:1051–1063.
- [14] Kamb WB. The thermodynamic theory of nonhydrostatically stressed solids. *J. Geophys. Res.* 1961;66:259–271.
- [15] Larché F, Cahn J. The effect of self-stress on diffusion in solids. *Acta Metall.* 1982;30:1835–1845.
- [16] Stephenson GB. Deformation during interdiffusion. *Acta Metall.* 1988;36:2663–2683.
- [17] Daruka I, Szabó I, Beke D, Cserhádi C, Kodentsov A, Van Loo F. Diffusion-induced bending of thin sheet couples: theory and experiments in Ti–Zr system. *Acta Mater.* 1996;44:4981–4993.
- [18] Nguyen T, Hubbard J, Pommersheim J. Unified model for the degradation of organic coatings on steel in a neutral electrolyte. *J. Coat. Technol.* 1996;68:45–56.
- [19] Prawoto Y, Kamsah N, Mat Yajid M, Ahmad Z. Energy density mechanics applied to coating blistering problems. *Theor. Appl. Fract. Mech.* 2011;56:89–94.
- [20] Prawoto Y, Onn IH. Application of J-integral concept on blister coating problem. *Eng. Fract. Mech.* 2012;92:114–125.
- [21] Cui Z, Gao F, Qu J. A finite deformation stress-dependent chemical potential and its applications to lithium ion batteries. *J. Mech. Phys. Solids.* 2012;60:1280–1295.
- [22] Yang F, Li J. Diffusion-induced beam bending in hydrogen sensors. *J. Appl. Phys.* 2003;93:9304–9309.
- [23] Rusanov AI. Surface thermodynamics revisited. *Surf. Sci. Rep.* 2005;58:111–239.
- [24] Wang W, Lee S, Chen J. Effect of chemical stress on diffusion in a hollow cylinder. *J. Appl. Phys.* 2002;91:9584–9590.
- [25] Xuan F-Z, Cao L-Q, Wang Z, Tu S-T. Mass transport in laser surface nitriding involving the effect of high temperature gradient: simulation and experiment. *Comput. Mater. Sci.* 2010;49:104–111.
- [26] Prawoto Y. Solid mechanics for materials engineers: principles and applications of mesomechanics. 2014. Available from: <http://www.amazon.com/MECHANICS-MATERIALS-Principle>
- [27] Nazir MH, Khan ZA, Stokes KA. Unified mathematical modelling and simulation for cathodic blistering mechanism incorporating diffusion and fracture mechanics concepts. *J. Adhes. Sci. Technol.* Forthcoming 2015. doi:10.1080/01694243.2015.1022496.

- [28] Nazir M, Khan Z, Stokes K. Modelling of metal-coating delamination incorporating variable environmental parameters. *J. Adhes. Sci. Technol.* 2014;1:29–32.
- [29] Saeed A, Khan Z, Clark M, Nel M, Smith R. Non-destructive material characterisation and material loss evaluation in large historic military vehicles. *Insight.* 2011;53:382–386.
- [30] Saeed A, Khan ZA, Hadfield M, Davies S. Material characterization and real-time wear evaluation of pistons and cylinder liners of the Tiger 131 military tank. *Tribol. Trans.* 2013;56:637–644.
- [31] Saeed A, Khan ZA, Montgomery E. Corrosion damage analysis and material characterization of sherman and centaur – the historic military tanks. *Mater. Perform. Char.* 2013;2:1–16.
- [32] Lu TQ, Zhang WX, Wang T. The surface effect on the strain energy release rate of buckling delamination in thin film–substrate systems. *Int. J. Eng. Sci.* 2011;49:967–975.
- [33] Sheeja D, Tay B, Leong K, Lee C. Effect of film thickness on the stress and adhesion of diamond-like carbon coatings. *Diamond Relat. Mater.* 2002;11:1643–1647.
- [34] Leterrier Y, Andersons J, Pitton Y, Manson JA. Adhesion of silicon oxide layers on poly (ethylene terephthalate). II: effect of coating thickness on adhesive and cohesive strengths. *J. Polym. Sci., Part B: Polym. Phys.* 1997;35:1463–1472.
- [35] Moody N, Venkataraman S, Nelson J, Worobey W, Gerberich W. Interface roughness effects on adhesion of Ta2N films. *Mat. Res. Soc. Symp. Proc.* 1993;327:337–342.
- [36] Sarikaya O. Effect of some parameters on microstructure and hardness of alumina coatings prepared by the air plasma spraying process. *Surf. Coat. Technol.* 2005;190:388–393.
- [37] Yagmur L. Effect of microstructure on internal friction and Young's modulus of aged Cu–Be alloy. *Mater. Sci. Eng. A.* 2009;523:65–69.
- [38] Fauchais P, Vardelle A. Thermal sprayed coatings used against corrosion and corrosive wear. In: Jazi H, editor. *Advanced plasma spray applications.* France: InTech; 2012. 250p. ISBN: 978-953-51-0349-3.
- [39] Moran MJ, Shapiro HN, Boettner DD, Bailey M. *Fundamentals of engineering thermodynamics.* New York, NY: Wiley; 2010.
- [40] Lewis GN. Outlines of a new system of thermodynamic chemistry. In: *Proceedings of the American Academy of Arts and Sciences.* Boston (MA): Metcalf; 1907. p. 259–293.
- [41] Li JC-M. Physical chemistry of some microstructural phenomena. *Metall. Trans. A.* 1978;9:1353–1380.
- [42] Li JC. High-angle tilt boundary – a dislocation core model. *J. Appl. Phys.* 1961;32:525–541.
- [43] Kellogg OD. *Foundations of potential theory.* New York (NY): Frederick Ungar; 1929.
- [44] Wang H. *Theory of linear poroelasticity with applications to geomechanics and hydrogeology.* Princeton (NJ): Princeton University Press; 2000.
- [45] Wang HF. *Theory of linear poroelasticity.* Princeton series in geophysics. Princeton (NJ): Princeton University Press; 2000.
- [46] Michaleris P, Dantzig J, Tortorelli D. Minimization of welding residual stress and distortion in large structures. *Weld. J. (NY).* 1999;78:361–366.
- [47] Lados DA, Apelian D, Wang L. Minimization of residual stress in heat-treated Al–Si–Mg cast alloys using uphill quenching: mechanisms and effects on static and dynamic properties. *Mater. Sci. Eng. A.* 2010;527:3159–3165.
- [48] Freund L, Floro J, Chason E. Extensions of the Stoney formula for substrate curvature to configurations with thin substrates or large deformations. *Appl. Phys. Lett.* 1999;74:1987–1989.
- [49] Klein CA. How accurate are Stoney's equation and recent modifications. *J. Appl. Phys.* 2000;88:5487–5489.
- [50] Hsueh C-H. Modeling of elastic deformation of multilayers due to residual stresses and external bending. *J. Appl. Phys.* 2002;91:9652–9656.
- [51] Zhang H, Davison W. Performance characteristics of diffusion gradients in thin films for the in situ measurement of trace metals in aqueous solution. *Anal. Chem.* 1995;67:3391–3400.
- [52] Cowper G. The shear coefficient in Timoshenko's beam theory. *J. Appl. Phys.* 1966;33:335–340.
- [53] David W, Thackeray M, De Picciotto L, Goodenough J. Structure refinement of the spinel-related phases $\text{Li}_2\text{Mn}_2\text{O}_4$ and $\text{Li}_{0.2}\text{Mn}_2\text{O}_4$. *J. Solid State Chem.* 1987;67:316–323.
- [54] Prussin S. Generation and distribution of dislocations by solute diffusion. *J. Appl. Phys.* 1961;32:1876–1881.

- [55] Zhang X, Shyy W, Marie Sastry A. Numerical simulation of intercalation-induced stress in Li-ion battery electrode particles. *J. Electrochem. Soc.* 2007;154:A910–A916.
- [56] Xuan F-Z, Shao S-S, Wang Z, Tu S-T. Influence of residual stress on diffusion-induced bending in bilayered microcantilever sensors. *Thin Solid Films.* 2010;518:4345–4350.
- [57] Hutchinson J, He M, Evans A. The influence of imperfections on the nucleation and propagation of buckling driven delaminations. *J. Mech. Phys. Solids.* 2000;48:709–734.
- [58] Hutchinson J, Thouless M, Liniger E. Growth and configurational stability of circular, buckling-driven film delaminations. *Acta Metall. Mater.* 1992;40:295–308.
- [59] Hutchinson JW. Mixed mode fracture mechanics of interfaces. *Metal Ceram. Interfaces.* 1990;4:295–306.
- [60] Collins JA. Failure of materials in mechanical design: analysis, prediction, prevention. New York (NY): Wiley; 1993.
- [61] Irwin GR. Fracturing of metals. Cleveland (OH): American Society of Metals; 1949. p. 147–166.
- [62] Hutchinson JW. Stresses and failure modes in thin films and multilayers. Lecture notes. 1996. Available from: <http://www.seas.harvard.edu/hutchinson/papers/462-5.pdf>
- [63] Schmauder S, Meyer M. Correlation between Dundurs' parameters and elastic constants. *Z. Metallkd.* 1992;83:524–527.
- [64] Sheen D. Introduction to numerical analysis. 1980. Available from: <http://www.osti.gov/eprints/topicpages/documents/record/784/0034855.html>
- [65] Mitchell AR, Griffiths DF. The finite difference method in partial differential equations. New York (NY): Wiley; 1980.
- [66] Brown D, Darr D, Morse J, Laskowski B. Real-time corrosion monitoring of aircraft structures with prognostic applications. In: Annual conference of the Prognostics and Health Management Society. Vol. 3. Minneapolis (MN): Prognostics and Health Management (PHM) Society; 2012. p. 1–12. Available from: http://www.phmsociety.org/sites/phmsociety.org/files/phm_submission/2012/phmc_12_018.pdf
- [67] Hartzell AL, Da Silva MG, Shea HR. MEMS reliability. New York (NY): Springer; 2011.
- [68] Parzen E. On estimation of a probability density function and mode. *Ann. Math. Stat.* 1962;33:1065–1076.